HHS Public Access

Author manuscript

Cell. Author manuscript; available in PMC 2024 May 11.

Published in final edited form as:

Cell. 2023 May 11; 186(10): 2160–2175.e17. doi:10.1016/j.cell.2023.04.010.

Structure-based Discovery of Conformationally Selective Inhibitors of the Serotonin Transporter

Isha Singh[†,1], **Anubha Seth**[2,†], **Christian B. Billesbølle**[1,†], **Joao Braz**[3,†], **Ramona M. Rodriguiz**[7,8], **Kasturi Roy**[2], **Bethlehem Bekele**[2], **Veronica Craik**[3], **Xi-Ping Huang**[4], **Danila Boytsov**[9], **Vladimir M. Pogorelov**[7], **Parnian Lak**[1], **Henry O'Donnell**[1], **Walter Sandtner**[9], **John J. Irwin**[1], **Bryan L. Roth**[4,5], **Allan I. Basbaum**[3,*], **William C. Wetsel**[7,8,10,*], **Aashish Manglik**[1,6,*], **Brian K. Shoichet**[1,*,#], **Gary Rudnick**[2,*]

[1.]Department of Pharmaceutical Chemistry, University of California San Francisco, 1700 4th St., Byers Hall Suite 508D, San Francisco, CA 94143, USA.

[2.]Department of Pharmacology, Yale University School of Medicine, 333 Cedar Street, New Haven, CT 06520-8066, USA.

[3.]Department of Anatomy, University of California San Francisco, San Francisco, CA 94143, USA.

[4.]Department of Pharmacology, NIMH Psychoactive Drug Screening Program, School of Medicine, University of North Carolina at Chapel Hill, Chapel Hill, NC 27599, USA.

[5.]Division of Chemical Biology and Medicinal Chemistry, Eshelman School of Pharmacy, University of North Carolina Chapel Hill, Chapel Hill, NC 27599, USA.

[6.]Department of Anesthesia and Perioperative Care, University of California, San Francisco, CA 94115, USA.

[7.]Department of Psychiatry and Behavioral Sciences, Duke University Medical Center, Durham, NC 27710, USA.

[8.]Mouse Behavioral and Neuroendocrine Analysis Core Facility, Duke University Medical Center, Durham, NC 27710, USA.

[*]Correspondence: Allan.Basbaum@ucsf.edu (A.B), william.wetsel@duke.edu (W.W), Aashish.Manglik@ucsf.edu (A.M), bshoichet@gmail.com (B.K.S), gary.rudnick@yale.edu (G.R).

[†]Contributed equally

[#]Lead contact.

Author Contributions: I.S, G.R and B.K.S designed the study. I.S launched the large-scale docking and performed hit to lead optimization. A.S, K.R and B.B experimentally tested the compounds in vitro. C.B.B solved the cryo-EM structure and interpreted the data. J.B, V.C conducted experiments in mice for anxiety and opioid withdrawal and interpreted the results. R.M.R, V.M.P and W.C.W conducted learned helplessness, tail suspension test, anti-depressive experiments and interpreted the results. X.P.H tested compounds for selectivity against other receptors. D.B and W.S collected the E-phys data on compounds. P.L and H.O.D collected aggregation data. W.S, J.J.I, B.L.R, A.I.B, W.C.W, A.M, B.K.S and G.R supervised the research. I.S, C.B.B, J.B, G.R, B.K.S and W.C.W wrote the manuscript along with input from all authors.

Declaration of Interests: B.K.S serves on the SAB of Schrödinger, Umbra Therapeutics, and Deep Apple; with J.J.I he co-founded Deep Apple Therapeutics and Blue Dolphin; with A.M and B.L.R he co-founded Epiodyne Ltd, while A.M also founded Stipple Bio and consults for Abolone and Septerna. W.C.W consults for Onsero Therapeutics, a company co-founded by B.L.R, who also serves on the SAB of Escient Pharmaceuticals and of Septerna. All other authors declare no competing interests.

[9]Institute of Pharmacology, Center for Physiology and Pharmacology, Medical University of Vienna, 1090 Vienna, Austria.

[10]Departments of Cell Biology, and Neurobiology, Duke University Medical Center, Durham, NC 27710, USA.

SUMMARY

The serotonin transporter (SERT) removes synaptic serotonin and is the target of anti-depressant drugs. SERT adopts three conformations: outward-open, occluded, and inward-open. All known inhibitors target the outward-open state except ibogaine, which has unusual anti-depressant and substance-withdrawal effects, and stabilizes the inward-open conformation. Unfortunately, ibogaine's promiscuity and cardiotoxicity limits understanding of inward-open state ligands. We docked over 200 million small molecules against the inward-open state of SERT. Thirty-six top-ranking compounds were synthesized and thirteen inhibited with further structure-based optimization leading to the selection of two potent (low nanomolar) inhibitors. These stabilized an outward-closed state of SERT with little activity against common off-targets. A cryo-EM structure of one of these bound to SERT confirmed the predicted geometry. In mouse behavioral assays, both compounds had anxiolytic- and anti-depressant-like activity, with potencies up to 200-fold better than fluoxetine (Prozac), and one substantially reversed morphine withdrawal effects.

Graphical Abstract

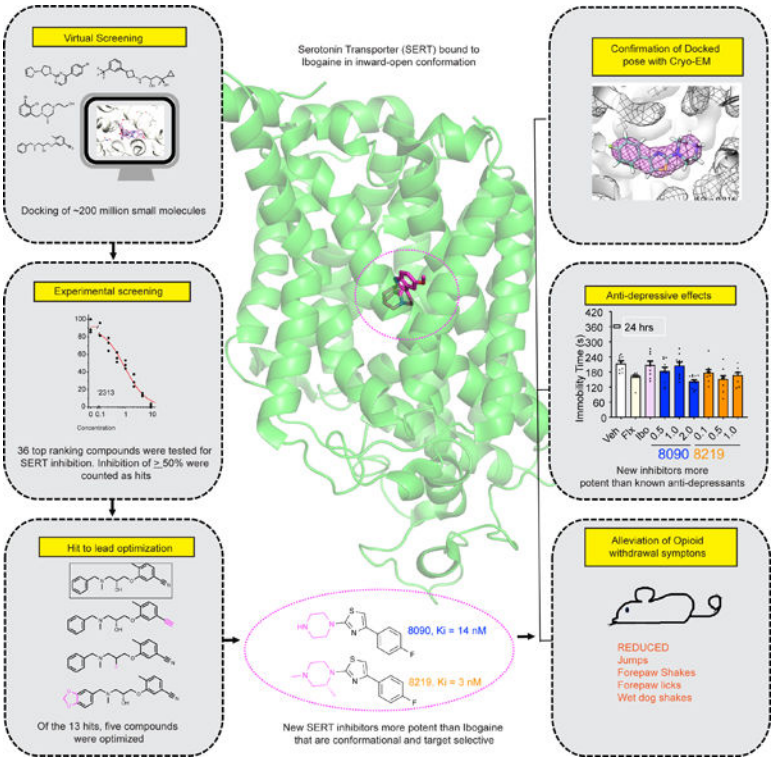

In Brief:

Development of low nM inhibitors conferring anti-depressant-like and anti-opioid withdrawal actions in mice from a large virtual library screened against the inward-open conformation of SERT.

INTRODUCTION

The serotonin transporter (SERT, SLC6A4) is the target of many drugs, including antidepressants and psychostimulants. Competitive inhibitors selective for SERT are widely used therapeutically to treat clinical depression. Examples include fluoxetine, citalopram and paroxetine (Prozac, Celexa and Paxil). [1] Cocaine, which also blocks the closely related transporters for norepinephrine and dopamine (NET and DAT), is a less selective competitive inhibitor for SERT [2]. In addition, ibogaine, and its metabolite noribogaine, are alkaloids that non-competitively inhibit SERT and DAT [3,4] but are much less selective, with affinity for many receptors and channels. [5]

SERT catalyzes re-uptake of serotonin (5-HT, 5-hydroxytryptamine) in a process that decreases the synaptic 5-HT concentration and recycles the neurotransmitter into the neuronal cytoplasm. In this process, which requires Na^+ and Cl^-, SERT cycles through distinct conformations. In the presence of extracellular Na^+, SERT is predominantly in an outward-open conformation. Binding of extracellular 5-HT and Cl^- allows conversion to an inward-open conformation before releasing bound Na^+ and 5-HT into the cell. Structures of SERT in these conformations obtained by X-ray crystallography and by cryogenic electron microscopy (cryo-EM) [6–8] align well to structures of other members of the NSS (neurotransmitter: sodium symporter), or SLC6 (solute carrier 6) gene families of transporters from both prokaryotes and animals [9–12] indicating a common conformational mechanism within the family.

In SERT and other NSS transporters, the observed conformations are related by conformational changes that open and close cytoplasmic and extracellular pathways to the central substrate site. Although conformational changes that open and close the pathways are coordinated, they are not strictly coupled, allowing multiple conformations of one pathway when the other pathway is closed. [10,13] Structural and functional studies show that Na^+ interacts with these transporters to close the cytoplasmic pathway and open the extracellular pathway, defining the outward-facing conformation. [14–20] Addition of substrate (and Cl^-, in the case of mammalian NSS transporters) closes the extracellular pathway and allows the cytoplasmic pathway to open [14,20–24], leading to the inward-open conformation.

In addition to Na^+, cocaine and antidepressants stabilize SERT in an outward-open conformation while ibogaine and noribogaine stabilize an inward-open conformation. [3,7,17,25] The opposing influence of these ligands on conformation mimics two functional states of SERT. The outward-facing SERT conformation with Na^+ but not 5-HT is like the conformation that cocaine stabilizes. SERT binds 5-HT, transports and releases it (along with Na^+) into the cytoplasm from an inward-open conformation – like the one stabilized by ibogaine. Return of SERT to an outward-facing state is much slower than the influx step[26] making the inward-open conformation predominant when SERT it is actively transporting 5-HT.

Ibogaine has unique behavioral properties, including reducing opiate withdrawal symptoms [27–30] and mitigating depression. [5,31] Given the opposite conformational responses of SERT to ibogaine and antidepressants [3,7,17,25], it's tempting to speculate that this conformational effect, as opposed to simply inhibiting 5-HT transport, contributes to ibogaine's unusual behavioral effects. This would be consistent with known effects of conformation on the transporter, such as the PKG-dependent phosphorylation of SERT Thr276. [23] Phosphorylation is enhanced by opening of the cytoplasmic pathway, which unwinds the region of TM5 containing Thr276, exposing it to the cytoplasm. [7] Agents that stabilize inward- or outward-facing SERT conformations increase or decrease phosphorylation, respectively, and transport of 5-HT also stimulates phosphorylation. [23] Thus, stabilizing a particular conformation may affect cellular signaling. Intriguingly, a mutation leading to dysfunctional Thr276 phosphorylation is associated with psychiatric disorders [32,33].

Confounding exploration of these ideas is ibogaine's profound target promiscuity [5], which clouds even SERT's role in ibogaine's behavioral effects. Accordingly, we sought compounds with effects on SERT akin to ibogaine's but acting with greater target selectivity. We used the cryo-EM structure of SERT complexed with ibogaine in an inward-open conformation [7] (PDB ID: 6DZZ) to computationally dock a library of over 200 million make-on-demand molecules. [34–37] Large library docking has revealed new ligands with high affinity and selectivity for several target families [34,37–63], though rarely transporters. From the docking against SERT, a diverse set of high-ranking compounds, physically complementing the inward-open state of SERT and topologically unrelated to previously known inhibitors, were prioritized for synthesis and biochemical testing. From an original set of actives, a cycle of structure-based design and testing led to two selective and potent compounds with anti-depressant-like and anxiolytic-like properties, that also act to reverse morphine withdrawal symptoms in mice, that inhibit SERT and close it extracellular pathway. A cryo-EM structure of one of these in complex with the transporter largely supports the docking-predicted geometry.

RESULTS

Retrospective control calculations.

The recent determination of the cryo-EM structure of the SERT-ibogaine complex in an inward-open state [7] afforded an opportunity to seek conformationally selective inhibitors. We targeted the extracellular-closed, inward-open state of the orthosteric site defined by residues such as Tyr95, Phe335 and Phe341. We further modeled two Na^+ ions and one Cl^- ion that contribute to transport [6,64] and for which sites are precedented in other transporter structures [9,11,65], though not explicitly seen in the ibogaine-SERT complex (Methods). We undertook retrospective control calculations against this site, seeking to confirm that we could preferentially dock ibogaine, noribogaine, 5-hyroxytryptamine (5-HT), cocaine, methylenedioxymethamphetamine (MDMA) and known selective serotonin reuptake inhibitors (SSRIs) [66] in favorable geometries with high complementarity versus a set of property matched decoys. [67] We further investigated whether ibogaine and noribogaine would dock preferentially to the inward-open versus the other SERT conformations. Results of these retrospective calculations supported an ability to capture known conformationally-

selective compounds in sensible geometries relative to property-matched decoys and to other states of the transporter.

Ultra-large library docking versus the inward-open conformation of SERT.

With the retrospective results in hand, we turned to docking a library of >200 million diverse, make-on demand molecules from the lead-like [68] subset of ZINC. [69] These molecules, with molecular weights <350 amu, cLogP values < 3.5, among other restrictions, have favorable physical properties that allow for further optimization. Each library molecule was sampled for physical complementarity to the inward-open state of SERT by DOCK3.7. [6,7] An average of 4358 orientations was sampled, and for each orientation about 187 conformations—over 1.57×10^{11} ligand configurations in total were sampled in 121,018 core hours (or 5 days over 1000 cores). High ranking molecules were filtered for interactions with Tyr95, Asp98, Tyr176, Ile172, Asn177, Phe335 and Phe335, those adopting strained conformations [70] were deprioritized, as were molecules that topologically resembled ~28,000 annotated aminergic ligands acting at serotonin, dopamine and adrenergic receptors as well as known inhibitors of SERT, DAT or NET with ECFP4-based Tanimoto coefficients (Tcs) ≤0.35, based on molecules annotated in ChEMBL20. [71] Of the remaining molecules, the top ranking 300,000 were clustered for similarity to one-another. The best scoring members of 5000 of the resulting clusters (top 0.002% of the docked library) were visually inspected for engagement with critical residues in the orthosteric pocket of inward-open state of SERT, and for any new interactions in the binding pocket, using Chimera. [72] These included salt bridge formation with Asp98, stacking with Phe335 and polar interactions with Asn177. Molecules with unsatisfied hydrogen bond donors and strained molecules were deprioritized. Ultimately, 49 molecules were selected for *de novo* synthesis and testing, out of which 36 were successfully synthesized (a 73.4% fulfillment rate). These 36 molecules are topologically both dissimilar to one another and dissimilar to known SERT inhibitors and complement the relatively unexplored inward-open state preferentially to the other two states seen to be adopted by SERT.

We first tested these 36 new compounds for SERT inhibition, beginning with the compounds at 30 μM (Figure 1A). Those molecules that inhibited ≥ 50% of [^{3}H]5-HT transport by SERT were considered active. Of the 36 tested, 13 molecules were active, a hit rate of 36% (hit rate = number-inhibited/number-tested) (Figure 1A, Table S1). This relatively high hit rate is noteworthy as this docking campaign is among the first of which we are aware against a transporter.

To verify that the inhibition of transport represented interaction with SERT, we tested the five most potent actives (ZINC000305339642 or **‘9642**, ZINC000623756919 or **‘6919**, ZINC000897222313 or **‘2313**, ZINC000417864931 or **‘4931** and ZINC000411862305 or ‘**2305**) for their ability to displace the cocaine analog 2β-carbomethoxy-3β-(4-iodophenyl)tropane (β-CIT, RTI-55), a high-affinity SERT inhibitor. In concentration-response these five inhibitors were well-behaved, displacing [^{125}I]β-CIT with affinities between 29 nM and 1.6 μM (Figure 1B, Table S2, chemical structures in Figure 1C). Docked poses of the five hits show unique interactions in SERT’s orthosteric site (Figure 1C).

Structure guided optimization.

We sought to improve the affinity of the five most active hits, representing 4 different chemotypes. Using the Smallworld (http://sw.docking.org) and Arthor (http://arthor.docking.org) search engines (NextMove Software, Cambridge UK) [69], substructure and similarity searches were conducted among >20 billion make-on-demand Enamine REAL molecules, seeking analogs that well-complemented the SERT site. In a second approach, analogs that tested the particular modeled interactions, such as the salt bridge with Asp98, and the π-π stacking with Phe341 and Ph335, were bespoke synthesized; these were unavailable among the make-on-demand sets. Between 15 to 23 analogs were synthesized and tested for each scaffold (Table S2). Encouragingly, the overall affinities of the analogs increased by 2- to 700-fold over the parent molecules, and four of the five scaffolds saw an improvement in affinity. Most promising were analogs of ZINC000897222313 (**‘2313**), which itself had a Ki of 0.92 μM, with ZINC000006658090 (**‘8090**) and ZINC000443438219 (**‘8219,** (*R*)-enantiomer) having Ki values of 14 nM and 3 nM, respectively (Figure 1D). In the docked poses of the parent lead and its optimized analogs **‘2313**, ‘**8090** and ‘**8219**, modifications to the piperazine ring led to better stacking with Phe335 and Tyr176 (Figure 1D–G). Consistent with the specificity of these interactions, the (*S*)-enantiomer of ‘**8219**, ZINC000443438221 (**‘8221**), which differs only in the stereochemistry of a piperazine methyl, had a Ki of 170 nM, something reflected in the poorer docking pose adopted by **‘8221**, which does not make a favorable hydrogen bond to the recognition Asp98, owing to packing flaws introduced by the methyl stereochemistry.

‘8090 and ‘8219 are not substrates.—Both **‘8090** and **‘8219** decreased the Vmax for 5-HT influx with minimal effect on KM, indicating non-competitive inhibition (Figure 2A), like ibogaine, an observation suggesting that they do not interfere with 5-HT binding from the external medium and are not substrates. To test this directly, we exploited an assay to measure SERT’s ability to exchange accumulated [^{3}H]5-HT with extracellular compounds. Extracellular unlabeled 5-HT, as a substrate, stimulated robust efflux of previously accumulated intracellular [^{3}H]5-HT as previously described [73,74] (Figure 2B). However, neither **‘8090** *nor* **‘8219** significantly increased efflux when added at saturating concentrations, further supporting the conclusion that they are not SERT substrates.

The effects of sodium and chloride ions on binding.—The compounds differ from ibogaine in their unique ionic requirements and effects on conformation. Ibogaine binding to SERT was *inhibited* by Na^+ and independent of Cl^-. [25] In contrast, binding of **‘8219**, measured by displacement of [^{125}I]β-CIT, was enhanced over 120-fold by Na^+ and over 9-fold by Cl^- (Figure 2C). For **‘8090**, these effects were smaller, with a 10-fold enhancement for Na^+ and a statistically insignificant effect of Cl^- (Figure S1). We also observed a decrease in affinity for both compounds in whole-cell transport measurements versus binding in membranes (Figure S1A). We note that have not observed such a decrease with other SERT inhibitors (see supplemental.pdf).

Effect on SERT conformation.—Because Na^+ and Cl^- influence the conformation of SERT and related transporters [20,23], we tested the effect of **‘8090** and **‘8219** on SERT conformation, seeking to understand if the new inhibitors stabilized the inward-open

conformation, as targeted and akin to ibogaine, the outward open conformation akin to cocaine and SSRIs, or an intermediate state. We used SERT mutants, depleted in reactive endogenous cysteine residues, and containing introduced cysteine residues in either cytoplasmic or extracellular pathways, as previously used to determine the conformational effects of ibogaine on SERT [75] (Figure S2). As expected, cocaine and ibogaine have opposing effects on the accessibility of this residue (Figure 3A). [75] Cocaine, by stabilizing SERT in an outward-open conformation, *decreased* Cys277 reactivity, versus control (no addition, dashed line), because the cytoplasmic pathway is closed in this conformation. [17] Conversely, ibogaine, by stabilizing SERT in an inward-open conformation, dramatically *increased* Cys277 reactivity.

To our surprise, neither **‘8219** nor **‘8090**, increased Cys277 reactivity and **‘8090** actually decreased reactivity slightly, though not nearly as much as cocaine (Figure 3A). In general, the effect of **‘8090** on the cytoplasmic pathway was similar to those of commonly used antidepressant compounds, and **‘8219** seemed not to affect the cytoplasmic pathway at all. However, these measurements were made in the presence of Na^+, which biases the conformation towards open-out by stabilizing the cytoplasmic pathway in a closed state. [18] In the absence of Na^+ (Figure 3B), **‘8219** increased Cys277 reactivity, versus control, indicating a more open cytoplasmic pathway in the absence of Na^+ (**‘8090** had no influence on the pathway). Because ibogaine, but not **‘8219** was able to overcome the effect of Na^+, we conclude that **‘8219** had a weaker influence but, like ibogaine, also stabilized the open state of the cytoplasmic pathway.

To complement these studies, we measured the effect of **‘8219** and **‘8090** on the reactivity of a cysteine replacing Tyr107 in the *extracellular* pathway. Cys107 in this SERT mutant reacts in the opposite way to Cys277 in the presence of cocaine and ibogaine; cocaine renders it more accessible and ibogaine decreases its accessibility. [75] Both **‘8090** and **‘8219** decreased Cys107 reactivity as ibogaine does, and unlike SSRIs (Figure 3C). [25]

Cryo-EM structure of a SERT/’8090 co-complex.

To test the docked model, we sought experimental structures of our optimized analogs in complex with SERT. Our attempts to obtain structures of SERT in the presence of K^+, which stabilizes the inward-open state used in our docking campaigns, were unsuccessful. We were able to determine a 3.0 Å structure of nanodisc-reconstituted [76] SERT bound to Fab15B8 [7] and compound ‘**8090** in the presence of Na^+ (PDB: 7TXT, EMBD: EMD-26160, Figures 4A and S3). The resulting map yielded well-defined and contiguous TM densities that allowed for unambiguous modeling of SERT regions important for ligand binding (Figure S3). A non-proteinaceous density overlapping with the orthosteric site, and with a local resolution of ~ 2.7 Å, allowed for confident modeling of **‘8090** (Figure 4A and Figure S3).

While Na^+ dramatically increased the affinity of **‘8219** and related compounds (Figures 2, 3, S1), our accessibility assays indicated that **‘8219** biases SERT toward an outward-closed state (Figure 3B, C). Taken together, our accessibility data likely reflect an equilibrium between open and closed states of the extracellular pathway induced by **‘8090**, similar to that reported for 5-HT bound SERT in Na^+. [8] However, exhaustive processing converged

on just a single structure of ‘**8090**-bound SERT in an outward-open conformation (1.43Å all-atom RMSD relative to paroxetine-bound SERT in an outward-open conformation, PDB ID:6VRH [7], with extracellular gating residues (Arg104 and Glu493; Tyr176 and Phe335) oriented to accommodate an extracellular solvent pathway reaching into the orthosteric site.

The experimental maps for **‘8090** broadly supports its docked binding pose, which occupies the SERT orthosteric site with key interacting residues Asp98, Tyr95 and Phe341, akin to the docking prediction (Figure 4). To compare like-to-like structures, **‘8090** was re-docked to the outward open conformation (PDB: 6DZY), where it achieved a docking score of −40.2 kcal/mol, very similar to its score of −40.9 kcal/mol against the inward-open conformation. In the outward-open conformation, the docked and cryo EM determined ligand superposed even more closely, with an RMSD value of 1.17 Å (Figure 4D, Supplementary Table S3 and Figure S3). In both the docked binding poses and cryo-EM fitted ligand, the compound ‘**8090** stacks with Phe341 and forms salt bridge with Asp98.

Both ‘8090 and ‘8219 are selective versus NET, DAT, and ~300 GPCR targets.

To compare inhibitory activity at neurotransmitter transporters, we tested compounds ‘**8090** and ‘**8219** in cell-based functional assays. Against DAT and NET, ‘**8090** had Ki values of 6.6 and 10 μM, respectively, while ‘**8219** had Ki values of 7 and 3.5 μM, respectively (Figure S4A−C). Both ‘**8090** and ‘**8219** were also tested for off-target agonist activity at > 300 human GPCRs in the Tango assay [77] at a concentration of 10 μM; little activity was seen against any target except for the 5-HT1A receptor. In concentration-response Gi activity assays, ‘**8090** had weak Gi agonist activity at 5-HT1A, with about 6% activity of reference agonist 5-HT (Figure S4D−F).

Mouse behavioral effects of ‘8090 and ‘8219.

Dysregulation of SERT is linked to major depressive disorder and SERT is the therapeutic target for many anti-depressants, including ibogaine, which is also reported to reduce substance withdrawal effects. With their favorable potency and apparently high selectivity, we were interested to test the new inhibitors for drug-like behavioral effects. Before doing so, it was important to investigate their exposure in the CNS on systemic dosing. Administering **8219** and **‘8090** at 10 mg/Kg intraperitoneal (i.p.) led to brain Cmax values of 3530 ng/g and 12000 ng/g with half-lives of 147 and 44.3 min, respectively (supplemental.pdf), relatively favorable exposure levels consistent with their small (<300 atomic mass units) and cationic nature, something for which they were explicitly selected in the docking and optimization.

‘8219 and ‘8090 have anti-depressive-like activities in genetically-modified and stressed mice.

The new inhibitors were tested for anti-depressive activities with wild-type (WT) and VMAT2 heterozygous (HET) mice, genetically-predisposed to depressive-like behavior, and with inbred C57BL/6J mice exposed to learned helplessness (LH) protocols to induce depressive-like behaviors. The basis for using the VMAT2 HET mice lies in a report that chronic inhibition of VMAT with reserpine in human hypertensive patients produced depression without anxiety [78]; thereby, providing a basis for the monoamine hypothesis

of depression. [79,80] The adult male and female VMAT2 HET mice are reported to be hypoactive in the open field, display anhedonia-like behavior with sucrose solutions, and show increased immobility in the forced swim and tail suspension tests that are alleviated with tricyclic anti-depressants, SSRIs, selective norepinephrine transporter inhibitors, and the atypical anti-depressant bupropion [81].

Tail suspension in VMAT2-HET mice.—Responses to a single administration of different doses of **‘8090** or **‘8219** were examined 30 min, 1, 7, or 12 days post-injection in VMAT2 mice (Figure 5), with 20 mg/kg fluoxetine (Flx) and 30 mg/kg ibogaine (Ibo) as controls. Immobility times in vehicle-treated VMAT2 HETs were prolonged significantly compared to WT controls at all time-points. Importantly, immobility times of the vehicle controls in both genotypes were stable over time—indicting no habituation in this test. Nevertheless, following acute administration, WT immobility times increased with Flx versus vehicle and with Ibo versus 1 mg/kg **‘8090** and 0.5 mg/kg **‘8219** (Figure 5A). Relative to vehicle, depressive-like responses in VMAT2 HETs were reduced with Flx, Ibo, 1 and 2 mg/kg **‘8090**, and 0.1 and 0.5 mg/kg **‘8219** (Figure 5B); 0.5 mg/kg **‘8219** was more efficacious than the same dose of **‘8090**. Notably, 0.1 mg/kg of **‘8219** was roughly equal in efficacy to 20 mg/kg of Flx – a 200-fold difference in potency.

Twenty-four h post-injection, in WTs 1 mg/kg **‘8090** significantly decreased immobility compared to 0.5 mg/kg (Figure 5C). In mutants, anti-depressant-like effects were maintained with 2 mg/kg **‘8090**, 0.5 mg/kg **‘8219**, and Flx (Figure 5D); Ibo effects were lost. By 7 and 12 days post-administration, the anti-depressant-like effects were lost.

Depressive-like behavior in the LH model: sucrose preference.—In the LH model, the compounds were dosed daily over 14 days in C57BL/6J males; subsequently, administration was continued throughout LH training and over the first 13 days of testing, followed by treatment-withdrawal (Figure 6A). Just prior to LH testing, mice given 2 or 5 mg/kg **‘8090** showed a significant preference for sucrose compared to vehicle (Figure 6B). Hence, the anhedonia-like behavior of the vehicle group was ameliorated by **‘8090**. Sucrose preference was maintained with 2 mg/kg **‘8090** on days 0, 3, and 7, with preference appearing in the 5 mg/kg group on day 7. By contrast, **‘8219** did not show significant efficacy. The reduced sucrose preference in the vehicle and **‘8219** groups was not due to decreased drinking since fluid consumption was similar among groups across days (supplemental.pdf).

In a separate cohort, animals were treated with the vehicle and 10 mg/kg Flx as outlined (Figure 6A, *top*). On day −2, the Flx-treated mice showed an enhanced preference for sucrose over that of the vehicle controls (Table S4). No group differences in fluid intake were found. Hence, controls showed anhedonia-like responses before testing. On day 0, one-half of the vehicle group remained on this treatment, whereas the remainder were given 40 mg/kg Ibo daily through test day 13 (Figure 6A, *bottom*). The Flx group continued with their treatment through day 13, then all groups were treatment withdrawn. Overall, the vehicle group showed a reduced sucrose preference compared to Ibo and Flx mice. Total fluid consumption was similar across days (supplemental.pdf). Thus, both Ibo and Flx increased overall sucrose preference at testing.

Learned helplessness: tail suspension.—Anti-depressive-like responses were assessed also by tail suspension (Figure 6A, *bottom*). Immobility remained high in vehicle controls throughout treatment (days 1–8) and on day 15 of treatment withdrawal (Figure 6C). Immobility times were reduced with both **‘8090** and **‘8219** on days 0, 1, and 3. The 5 mg/kg **‘8219** remained efficacious to day 8 and over the first two days of treatment withdrawal (days 14 and 15). Since drugs that increase motor activity can confound these results, locomotion was examined; no effects were observed (supplemental.pdf). Thus, both **‘8090** and **‘8219** exert anti-depressant activities in tail suspension.

The vehicle, Ibo, and Flx groups were tested also in tail suspension (supplemental.pdf). On the first 2 days of testing, immobility times were high in the vehicle controls relative to Ibo and Flx mice and, for Flx, this effect was maintained through day 3. By day 8, significant group differences were lost, but upon treatment-withdrawal immobility was enhanced in the Ibo and Flx groups. No locomotor differences were found (supplemental.pdf). In summary, both **‘8090** and **‘8219** maintain anti-depressive-like actions throughout testing and effects of **‘8219** persist in early withdrawal. Ibo and Flx anti-depressant-like activities are transient and upon withdrawal immobility is increased.

Learned helplessness: shock escape.—Assessment of shock-escape performance revealed the numbers of escapes in vehicle controls relative to the compound treatments remained low during LH training (days −9 and −2), at testing with compounds (days 4 and 10), and upon treatment withdrawal (days 18 and 23) (Figures 6A and S5A). On days 10 and 23, shock-escape performance increased over vehicle with 5 mg/kg **‘8090** and **‘8219**. On day 23 performance was higher also in the 1 mg/kg **‘8090** group than controls. Escape latencies showed a similar picture (Figure S5B). Here, 5 mg/kg **‘8219** was efficacious on day 4 during treatment and during treatment withdrawal on day 23. As a control, sensitivity to foot-shock was evaluated during treatment day 13 and treatment-withdrawal day 23 (Figure 6A, *bottom*). On day 13 intensity-dependent responses were evident, whereby on day 22 all mice were more responsive to the 0.3 mAmp foot-shock. Together, our results indicate that the new inhibitors promote shock-escape performance.

For the vehicle and Flx mice, no differences were noted in the numbers and latencies to escape during conditioning days −9 and −2 (Table S5). Nevertheless, at testing the numbers of escapes were depressed in the vehicle controls (Figure S6A) and the escape latencies were prolonged relative to the Flx and Ibo mice (Figure S6B). With respect to sensitivity to foot-shock, no treatment effects were observed (Figure S6C). Collectively, **‘8090** and **‘8219**, as well as Ibo and Flx do not affect reactivity to foot-shock, whereas they improve shock-escape performance.

Learned helplessness: anxiety and working memory.—In the elevated zero maze, LH mice given 2 or 5 mg/kg **‘8090** or 5 mg/kg **‘8219** spent more time and entered the open areas more readily than vehicle-treated mice displaying an anxiolytic drug-like effect (supplemental.pdf). While motor activities were similar among animals receiving the compounds, locomotion in the maze was increased with 5 mg/kg **‘8090** versus vehicle (supplemental.pdf). This difference probably exerted no effect on their anxiety-like

responses since the open area times and latencies to enter the arms were virtually identical among the **‘8090** and **‘8219** groups (supplemental.pdf).

Flx increased open area time compared to Ibo and vehicle controls, whereby no significant differences were found for the latency to enter the open areas. However, locomotor activity was decreased by Ibo (supplemental.pdf). Since alterations in locomotion can confound time spent in and latency to enter the open areas, we controlled these differences with ANCOVA. Here, only percent time in the open areas was enhanced in the Flx-treated mice relative to the vehicle controls. In summary, both **‘8090** and **‘8219**, and Flx showed anxiolytic actions in the elevated zero-maze.

We also assessed ‘**8219** and ‘**8090 (**10 mg/kg/day for 10 days) in the elevated plus-maze test of anxiety. Compared to vehicle both inhibitors increased the percentage of entries into and the time spent exploring the open arms (supplemental.pdf). Importantly, neither total entries into all arms nor total distance travelled over the 5 min test period differed between the groups, indicating that these inhibitors did not alter motor performance and/or exploratory behavior. As expected, compared to vehicle, mice that received a control SSRI, paroxetine (10 mg/kg), also spent more time exploring the open arms (supplemental.pdf). Thus ‘**8219** and ‘**8090** exert anxiolytic-like effects comparable to paroxetine.

In patients and animal models, depression can impair working memory [82]. In the 8-arm radial maze, the numbers of spontaneous novel arm selections were similar among groups before re-visiting an arm for the first time (Figure S7A). Nevertheless, the 2 mg/kg **‘8090** or 5 mg/kg **‘8219** groups recognized this error more readily than vehicle controls, since they entered more arms before making a second repeated entry (Figure S7C). Importantly, this enhanced working memory cannot be attributed to increased exploration since all groups traveled similar distances within the maze (Figure S7E).

For mice treated with the vehicle, Ibo, or Flx, Ibo suppressed locomotion (Figure S7F). Hence, ANCOVA was applied to the first and second entries to repeat. Here, the Flx mice entered more arms before repeating a first entry compared to Ibo and vehicle mice (Figure S7B). However, the converse was true for the repeated second entry for the vehicle-versus the Flx-treated animals (Figure S7D). Thus, Flx is most efficacious in improving working memory early in testing, whereas **‘8090** and **‘8219** are most efficacious later.

The new SERT inhibitors reduce opioid withdrawal symptoms.

Given ibogaine’s use to treat opioid withdrawal [27–30], we investigated ‘**8219** effect on opioid withdrawal. We treated mice for 4 days with escalating doses of morphine (10 to 75 mg/kg). On the fifth day, the mice received a single dose of morphine (20 mg/kg) followed either by vehicle, ‘8219 (10 mg/kg), or paroxetine (10 mg/kg), and finally followed by naloxone-precipitated withdrawal (10 mg/kg). As expected, paroxetine significantly reduced naloxone-precipitated jumps and rearings [83,84] (Figure 7). In contrast, ‘**8219** not only reduced jumps, but also decreased forepaw and wet-dog shakes. We conclude that ‘**8219** is as good if not better than paroxetine at mitigating opioid withdrawal symptoms and likely better than ibogaine, whose SERT activity is clouded by broad polypharmacology.

DISCUSSION

From large-library docking against the inward-open conformation of SERT emerged chemotypes with new pharmacology. In this still rare campaign against a transporter, the docking hit rate was high at 36%, as was the potency of the initial top-ranking molecules, many of which had sub-μM to even mid-nM Ki values. All of these compounds represent new chemotypes, topologically unrelated to known SERT inhibitors in the IUPHAR [85,86] or ChEMBL [71] databases. The compounds were also selective for SERT (Figure S4), with little meaningful activity against well-known off-targets such as NET, DAT, and the serotonergic GPCRs, in contrast with the broad promiscuity of ibogaine [5]. This study thus supports the plausibility of targeting transporters for structure-based discovery. Several other observations merit emphasis. First, the new chemotypes appear to exert unique influences on transporter conformation, closing the extracellular pathway and not opening the intracellular pathway except (for **‘8219**) in the absence of Na^+. How much this reflects the targeting of the inward-open state, against which the molecules were selected, and how much this reflects simply the unusual chemotypes, is unclear, but it does present opportunities for new functional outcomes. Second, structure-based optimization improved potency, with the best molecule inhibiting SERT with Ki value of 3 nM. Third, the cryo-EM structure of the SERT-**’8090** complex, while captured in the outward-open conformation, perhaps reflecting the conformational influence of Na^+, broadly confirms the docked-predicted pose, with the inhibitor’s binding pose overlapping closely with the transporter’s central 5-HT site [8] and making predicted interactions, including with Asp98, Phe341, Phe335 and Y176 in both the inward- and outward-open conformations. Finally, the compounds were selected for favorable physical properties and have high brain exposure. This contributes to their potent activity in mouse anxiolytic and especially anti-depressant assays; in the latter, the new inhibitors were as much as 200-fold more potent than Flx; this activity may reflect both their unprecedented chemotypes and the transporter states that they stabilize.

Limitations of the Study.

Certain caveats should be mentioned. The large-scale docking was launched against the inward-open state conformation of SERT, seeking compounds that phenocopied ibogaine on SERT, but with higher target selectivity. Such compounds would allow testing the hypothesis that the unique conformational effect of ibogaine might be responsible for its reported ability to ameliorate opiate withdrawal [27–30] and depression. [5,31] Our most potent ligands were not purely selective for this conformation, instead seeming to selectively stabilize a state in which the extracellular pathway is closed—as modeled—but the inward pathway is hardly changed. Moreover, the ligands differed markedly from ibogaine in their response to Na^+ and Cl^- (Figures 2C, S1). While the docking predicted structure interacts with the same residues and certainly the same overall site as that observed in the *outward*-open cryoEM structure, the superposition is only approximate, with an RMSD of 2.11 Å in ligand atoms (this improves to 1.17 Å when comparing the cryoEM structure with a docking to the outward-open conformation, Figure 4D). We do note that even ibogaine, which strongly stabilizes inward-open/outward-closed states, binds not only the inward-open state but also the outward-open and occluded states, reflecting overall similarities of the orthosteric sites in all three conformations. [7] Despite these differential effects on SERT conformation, **‘8219**

and **‘8090** phenocopy ibogaine’s reported effects on opioid withdrawal and depression, and these effects are distinguishable from those of SSRIs, which inhibit SERT in a different conformation.

These cautions should not obscure the major observations from this study. Large library docking against the inward-open conformation of SERT discovered 13 new compounds representing 12 chemotypes that bound to the transporter with low μM to mid-nM concentrations. The docked structures templated optimization to the low nM range. As observed against other flexible targets [35,37,50], the new chemotypes conferred new *in vitro* activities that likely contributed to the unusually high efficacy of the new SERT inhibitors in animal models of depressive-like responses. Indeed, the selectivity of the new SERT inhibitors versus off-targets like NET, DAT, and serotonergic GPCRs, and for a particular SERT conformational state, may make them useful as tool molecules to probe transporter function and therapeutic translation. Accordingly, we are making them openly available via the Millipore-Sigma probe collection. Finally, this study supports the pragmatism of structure-based campaigns against transporters and suggests that even for those as intensely studied as SERT, new structures can template the discovery of potent new chemotypes, conferring new pharmacology.

STAR METHODS

RESOURCE AVAILABILITY

Lead Contact—Further information and requests for resources and reagents should be directed to and will be fulfilled by the Lead Contact, Brian K. Shoichet (bshoichet@gmail.com)

Materials availability—The following plasmids used in this study have been deposited to Addgene: SERT WT, www.addgene.com/190743; SERT C109A_Y107C, www.addgene.com/190174; SERT X5C_S277C www.addgene.com/190177

Data and code availability

Data.: All data reported in this paper will be shared by the corresponding authors upon request. The cryoEM structure of 8090 in complex with SERT has been deposited in the PDB (7TXT). The docking program used in this study is available without cost for academic research (https://dock.compbio.ucsf.edu/DOCK3.7). A web-based version of this method is available to all for all uses via https://blaster.docking.org/. The molecular database screened in this study is openly available to all at https://zinc20.docking.org/.

Code.: This paper does not report original code.

Any additional information required to reanalyze the data reported in this work is available from the Lead Contact upon request.

EXPERIMENTAL MODEL AND SUBJECT DETAILS

Cell lines.—HeLa cells were obtained from ATCC and cultured under their recommended conditions. The cells used have not been otherwise authenticated.

Animals.—Animal experiments were conducted under protocols approved by the UCSF and Duke University Institutional Animal Care and Use Committees in accordance with the NIH Guide for the Care and Use of Laboratory Animals. Adult (2–3 mos) male C56BL/6J mice were purchased from the Jackson Laboratory (strain #000664) and used in the plus maze and opioid withdrawal studies at UCSF, while all other behavioral experiments were conducted at Duke. Adult (4–6 mos) male and female wild-type (WT) and vesicular monoamine transporter 2 (VMAT2) heterozygous (HET) mice were used in the tail suspension studies. All mice were housed 3–4 in cages, in a humidity and temperature-controlled room, on a 12:12 h light/dark cycle (UCSF) or on a 12:12 h light/dark cycle (lights on 0600 h; Duke) with food and water provided *ad libitum*, unless noted otherwise.

METHOD DETAILS

Molecular Docking—Serotonin transporter bound to ibogaine in an inward-open conformation [7] (PDB ID: 6DZZ) was used for docking a library of >200 million “lead-like ” molecules from the ZINC20 database (http://zinc20.docking.org) using DOCK3.7 [87]. Forty five matching spheres or local hot-spots generated from the cryo-EM pose of ibogaine were used in the binding site for superimposing pre-generated flexible ligands and the poses were scored by summing the van der waals interaction energies, receptor-ligand electrostatics and ligand desolvation energies [88,89]. The receptor atoms were protonated with Reduce [90] and partial charges calculated using united-atom AMBER force field [91]. AMBER force field was also used for pre-generation of energy grids using QNIFFT [92,93] for Poisson–Boltzmann-based electrostatic potentials, CHEMGRID [94] for van der Waals potential, and SOLVMAP [88] for ligand desolvation.

The docking setup was optimized for its ability to enrich knows SERT binders including ibogaine, noribogaine, 5-hyroxytryptamine (5-HT), cocaine and known selective serotonin reuptake inhibitors (SSRIs) [66], in favorable geometries with high complementarity versus a set of property matched decoys [67]. About 50 decoys were generated for each ligand that had similar chemical properties to known ligands but were topologically dissimilar. The best optimized docking setup was evaluated using enrichment of ligands over decoys using log-adjusted area under the curve (logAUC values). The best docking setup was able to enrich the cryo-EM pose of ibogaine as well as dock other known ligands in the right conformation. All docked ligands were protonated with Marvin (version 15.11.23.0, ChemAxon, 2015; https://www.chemaxon.com) at pH 7.4, rendered into 3D with Corina (v.3.6.0026, Molecular Networks GmbH; https://www.mn-am.com/products/corina), and conformationally sampled using Omega (v.2.5.1.4, OpenEye Scientific Software; https://www.eyesopen.com/omega). Before launching a screen of >200 million make-on demand lead like molecules, an ‘extrema set’ of 61,687 molecules was docked in the optimized system to ensure that the molecules with correct physical properties were enriched.

Overall, in the prospective screen, each library molecule was sampled in about 4358 orientations, on average about 187 conformations were sampled over 5 days on 1000 cores. The top-ranking 300,000 molecules were filtered for novelty using ECFP4-based Tanimoto coefficient (Tc <0.35) against known inhibitors of SERT, DAT or NET and ~28,000 annotated aminergic ligands acting at serotonin, dopamine and adrenergic receptors

in ChEMBL [71]. The remaining molecules were further clustered by an ECFP4-based Tc of 0.5. From the top 5,000 novel chemotypes, strained molecules with >2 kcal mol−1 internal strains were filtered out and the rest were visually inspected for the best docked poses with favorable interactions with the SERT active site, including salt bridge formation with Asp98, pi-pi stacking with Phe335 or Phe341 and polar interactions with Asn177. Ultimately, 49 molecules were selected for de novo synthesis and testing, out of which 36 were successfully synthesized and tested.

Hit to lead optimization—Using 5 primary docking hits ‘9642, ‘6919, ‘2313, ‘4931 and ‘2305 as queries in SmallWorld (https://sw.docking.org/) and Arthor (http://arthor.docking.org) search engines (NextMove Software, Cambridge UK) [69], substructure and similarity searches were conducted among >20 billion make-on-demand Enamine REAL molecules. The resulting analogs were further filtered based on Tc > 0.4 and docked to the SERT inward open active site. The docked poses were visually inspected for compatibility with the site, including salt bridge formation with Asp98, pi-pi stacking with Phe335 or Phe341 and polar interactions with Asn177 and prioritized analogs were synthesized and experimentally tested.

Make-on-demand synthesis and Compound Handling—49 molecules from the large scale prospective docking were delivered within 5 weeks with a 73.4% fulfillment rate after a single synthesis attempt. These make-on demand molecules were derived from the Enamine REAL database (https://enamine.net/compound-collections/real-compounds). Portions of each compound (1 to 2 mg) were dissolved in DMSO at a concentration of 10 mM and stored as stock solutions at −20° C. The rest of the dry powder was also stored at −20° C for additional rounds of testing. Freeze-thaw cycles were minimized.

Transport and efflux measurements for Screening and Characterization—5-HT transport into RBL cells or SERT-transfected HeLa cells was measured as described previously [95]. Briefly, cells growing in 48- or 96-well plates were washed once with 100 µl (200 µl for 48-well plates) of PBS/CM (phosphate-buffered saline containing 0.1 mM CaCl2 and 1 mM MgCl2). 5-HT uptake assays were initiated by the addition of [^{3}H]5-HT (20 nM final concentration) and unlabeled 5-HT to the indicated total concentration (for determination of KM and Vmax). The assays were terminated after 10 min by three rapid washes with ice-cold PBS. The cells were then solubilized in 30 µl (150 µl for 48-well plates) of 0.01 M NaOH for 30 min. For 96-well assays, 120 µl of Optifluor (Perkin-Elmer) was added and accumulated [^{3}H]5-HT was determined by liquid scintillation spectrometry in a PerkinElmer Microbeta plate counter. For 48-well assays, the NaOH-lysed cells were transferred to scintillation vials with 3 ml of Optifluor and counted by liquid scintillation spectrometry. For efflux experiments (in 48-well plates, incubations with 20 nM [^{3}H]5-HT were extended to 15 min, followed by 2 washes with PBS/CM, and further incubation in 200 µl PBS/CM with or without the indicated inhibitor. Incubations were terminated as above at 5 min intervals up to 20 min and counted. Time courses were fitted by linear regression of the time courses.

Binding measurements—Binding of the high-affinity cocaine analog [^{125}I]β-CIT was measured in crude membrane preparations from SERT-transfected HeLa cells as described previously [95]. For membrane binding assays, frozen membranes from cells expressing SERT mutants were thawed on ice, applied to Multiscreen-FB 96-well filtration plates (Millipore, approximately 100 μg per well), and washed five times by filtration with 100 μl of binding buffer (10 mM HEPES buffer, pH 7.4, containing 150 mM NaCl, Na-isethionate, or NMDG-Cl as indicated). β-CIT binding was then initiated by the addition of 100 μl of binding buffer containing 0.1 nM [^{125}I]β-CIT and the indicated concentration of individual test compounds. Binding was allowed to proceed for 1.5 h at 20°C with gentle rocking. The reaction was stopped by filtration and three washes with 100 μl of ice-cold PBS buffer. 50 μl of Optifluor was added to each filter and the plates were counted with a PerkinElmer Microbeta plate counter.

Accessibility measurements—Conformational changes were measured using the accessibility of cysteine residues placed in the cytoplasmic (S277C) and extracellular (Y107C) permeation pathways as described [3]. For measuring extracellular pathway accessibility, intact cells expressing SERT C109A-Y107C growing in 96-well plates were incubated for 15 min with 0.01–10 mM MTSET in the presence or absence of test compounds and then washed with PBS/CM. Transport rates were then measured to determine the reactivity of Y107C under the experimental conditions tested. For cytoplasmic pathway accessibility, membranes prepared from cells expressing SERT S277C-X5C were applied to Multiscreen-FB 96-well filtration plates, washed as in the binding assays, and then incubated for 15 min with 0.01–1 mM MTSEA in the presence or absence of test compounds. and then washed with PBS/CM. Binding of the high affinity cocaine analog β-CIT was measured on the filters as described above. Modification of Cys277 inactivates β-CIT binding by preventing closure of the cytoplasmic pathway and opening of the extracellular pathway [96]. For measurements with both transport and binding, the concentration of MTSEA or MTSET leading to half-maximal inactivation were used to calculate the rate constant for inactivation and expressed either as that rate constant or the rate relative to the control rate in the absence of test compound. All test compounds and other inhibitors were added at 10x the KI measured for inhibition of binding or transport, depending on the assay. In some cases, particularly in the assays with intact cells, incomplete washout of inhibitors prevented accurate assessment of the sensitivity to MTS reagents. In those cases, the inhibitor concentration was lowered until the residual activity after washing was sufficient to make accurate measurements. In no case was inhibitor concentration decreased lower than the IC50 for transport inhibition.

Dissociation measurements—Dissociation rates for **‘8090** and **‘8219** were determined under whole-cell patch clamp by first inhibiting SERT with a saturating concentration of the inhibitor and then washing the inhibitor away while testing for recovery of SERT currents by frequent application of 5-HT. HEK293 monoclonal cells stably expressing GFP-hSERT were incubated for 2h with 75nM and 50nM of **‘8090** and **‘8219** respectively in an external solution (140mM NaCl, 3mMKCl, 2.5mM CaCl2, 2.0mM MgCl2, 10mM HEPES pH 7.4, 20mM glucose). Patch-clamp pipettes were back-filled with an internal solution (133 mM K-MES, 1.0mM CaCl2, 0.7mM MgCl2, 10mM EGTA, 10mM HEPES pH 7.2). Patched

cells were constantly perfused for 37.5min with an inhibitor-free external solution. A 1s pulse of 10μM 5-HT was applied to the cell every 15s during this perfusion. The amplitude of 5-HT induced steady-state current [97] was recorded and plotted vs. time.

Neurotransmitter Transporter Assays for Determining Selectivity—DAT, NET, and SERT activities were determined using the neurotransmitter transporter update assay kit from Molecular Devices (Category R8174). Briefly, HEK293 cells stably expressing human DAT, NET, or SERT were plated in Poly-L-Lys (PLL) coated 384-well black clear bottom plates in DMEM supplemented with 1% dialyzed FBS (dFBS), at a density of 15,000 cells in 40 μl per well. After overnight recovery, the cells were removed of medium, received 25 μl per well drug solutions prepared in assay buffer (1x HBSS, 20 mM HEPES, pH 7.40, supplemented with 1 mg/ml BSA) for 30 min at 37°C, followed by 25 μl per well of dye solution for an additional 30 min incubation at 37°C. Cocaine, Nisoxetine, and fluoxetine served as positive controls for DAT, NET, and SERT, respectively. Fluorescence intensity was measured on the FlexStation II with excitation at 440 nm and emission at 520 nm. Relative fluorescence units (RLU) were exported and analyzed in Prism 9.0.

GPCRome screening assays—Off-target agonist activity at human GPCRome was carried out using the PRESTO-Tango assays as described before [77] with modifications. In detail, HTLA cells were plated in PLL coated white clear-bottom 384-well plates in DMEM supplemented with 1% dFBS, at a density of 10,000 cells in 40 μl per well. After recovery for about 6-hour, the cells were transfected with 20 ng DNA per well for overnight incubation, followed by addition of 10 μl of selected test compounds, prepared in DMEM supplemented with 1% dFBS. The cells were incubated with drug overnight (usually 16 – 20 hours). Medium and drugs were then removed and 20 μl per well of BrightGlo reagents diluted in assay buffer were added. Plates were incubated for 20 min at room temperature in the dark and luminescence was counted. In each plate, the dopamine receptor D2 was included as an assay control and was stimulated with 100 nM of the agonist quinpirole. Each receptor had 4 replicate wells of basal (with medium) and 4 replicate wells of sample (10 μM final in this case). Results were expressed in as fold change over average basal.

GPCR β-Arrestin Tango Assays—HTLA cells were transfected with target receptor construct in DMEM supplemented with 10% FBS for overnight, plated in PLL coated white clear-bottom 384-well plates in DMEM supplemental at a density of 10,000 cells in 40 μl per well. After recovery for about 6-hours, compound in serial dilutions, prepared in DMEM supplemented with 1% dFBS, were added to cells, 10 μl per well in 5x of the final designed. The plate was incubated overnight, usually 16 – 20-hours and luminescence counts were determined as above. Results were analyzed and processed in Prism 9.0.

GloSensor cAMP Assays—HEK293 T cells were co-transfected with the target receptor construct and GloSensor cAMP reporter (Promega) in DMEM supplemented with 10% FBS for overnight incubation. Transfected cells were plated in PLL coated white clear-bottom 384-well plates in DMEM supplemented with 1% dFBS at a density of 15,000 to 20,000 cells in 40 μl per well. After recovery of a minimum of 6-hours (up to 24-hours), cells were used for GloSensor cAMP assays. Briefly, cells were removed of medium and received

25 μl per well compound solutions, prepared in assay buffer (1x HBSS, 20 mM HEPES, pH 7.40, supplemented with 1 mg/ml BSA) supplemented with 4 mM luciferin. For Gs agonist activity, the plates were counted for luminescence after 20 min incubation at room temperature in the dark. For Gi agonist activity, 10 μl of isoproterenol (ISO at a final of 100 nM, used to activate endogenous ß2-receptors to activate Gs and then adenylyl cyclase activity) was added at 15 min after compound and the plate was counted after 20 min as above. Results were analyzed in Prism 9.0.

Expression and purification of SERT and Fab15B8—The ΔN72/ΔC13 N- and C-terminally truncated human wild-type SERT amino acid sequence [7] was codon optimized and synthesized (Twist Bioscience). The SERT gene (*Slc6a4*) fragment was cloned into a pcDNA3.4-zeocin-TetO vector with a C-terminal human rhinovirus 3C cleavage site, followed by a human protein C tag (EDQVDPRLIDGK), and a 10 x polyhistidine tag. Expi293F cells at 3.0×10^6 cells/ml were transfected with 1 μg DNA per ml culture using the Expi293 Expifectamine kit (Life Technologies) according to the manufacturer's recommendations. The following day, expression was induced with 1 μg/ml doxycycline hyclate (Sigma Aldrich), and Expifectamine Enhancer Solutions I and II (Life Technologies) were added. After 48 h cells were harvested by centrifugation at 4,000 x *g*, and stored at −80°C until further use. On the day of purification, cells were thawed and dounce homogenized into ice cold solubilization buffer comprised of 100 mM NaCl, 20 mM HEPES pH 7.50, 1% (w/v) DDM, 0.1% (w/v) CHS, EDTA-free protease inhibitor (Thermo Fisher), and 30 μM compound **'8090**. Cells were solubilized for 60 min at 4°C and centrifuged at 14,000 x g for 30 min at 4 C. The supernatant was supplemented with 2 mM CaCl2 and loaded over homemade anti-protein C affinity resin. The resin was washed with 25 C.V. of buffer comprised of 100 mM NaCl, 20 mM HEPES pH 7.50, 0.1% (w/v) DDM 0.01% (w/v) CHS, 1 mM CaCl2, and 10 μM **'8090**. SERT was eluted with 100 mM NaCl, 20 mM HEPES pH 7.50, 0.1% (w/v) DDM 0.01% (w/v) CHS, 1 mM EDTA, 0.2 mg/ml protein C peptide (Genscript), and 30 μM **'8090**.

Fab15B8 heavy and light chain amino acid sequences were obtained from the literature [7] and codon optimized genes were designed with an N-terminal H7 signal sequence and a C-terminal polyhistidine tag. The genes were synthesized and cloned into the commercially available pTWIST-CMV expression vector (Twist Bioscience). Expi293F cells at 3.0×10^6 cells/ml were transfected with 1 μg total DNA per ml culture of heavy chain and Light chain DNA in a 2:1 mass ratio, using the Expi293 Expifectamine kit (Life Technologies). The following day, Expifectamine Enhancer Solutions I and II (Life Technologies) were added. At approximately 120 h, culture was harvested by centrifugation at 4,000 x *g* and the supernatant containing Fab15B8 was loaded over a Ni-NTA column. The column was extensively washed with 20 mM HEPES pH 7.50, 100 mM NaCl, 30 mM imidazole. Fab15B8 was eluted with 20 mM HEPES pH 7.50, 100 mM NaCl, 250 mM imidazole, concentrated on a 10k MWCO spin filter (Amicon), and aliquots were flash frozen in liquid N2 and stored at −80°C until use.

Nanodisc-SERT reconstitution—Approximately 150 μg of purified SERT was reconstituted into lipidic nanodiscs by mixing with purified MSPNW11 and a lipid

mixture containing 2:3 weight ratio of 1-palmitoyl-2-oleoylphosphatidylcholine (POPC, Avanti) and 1-palmitoyl-2-oleoyl-*sn*-glycero-3-phospho-(1′-rac-glycerol) (POPG, Avanti). A SERT:MSPNW11:lipid molar ratio of 1:20:800 was used in buffer comprising 20 mM HEPES pH 7.50, 100 mM NaCl, 1 mM EDTA, 30 μM **‘8090**. MSPNW11 was purified as described previously [98]. Samples were incubated under slow rotation for 1 h at 4°C. Detergent was removed by addition of 200 mg/ml SM-2 BioBeads (BioRad) followed by incubation under slow rotation for 16 h at 4°C. The reconstituted sample was separated from BioBeads and 2 mM CaCl2 was added before loading over an anti-protein C affinity resin. The resin was washed with 100 mM NaCl, 20 mM HEPES (pH 7.50), 1 mM CaCl2 and 10 μM **‘8090**. Nanodisc-SERT was eluted with 100 mM NaCl, 20 mM HEPES pH 7.50, 0.5 mM EDTA, 0.2 mg/ml protein C peptide (Genscript), and 30 μM **‘8090**. The nanodisc-SERT sample was concentrated using a 50k MWCO spin filter (Amicon).

Cryo-EM sample preparation and data collection—Nanodisc reconstituted SERT was mixed with 1.25 fold molar excess purified Fab15B8 and incubated 30 min on ice. The complex was purified by size exclusion chromatography (SEC) on a Superdex S200 Increase 10/300 GL column (GE Healthcare) into buffer comprised of 100 mM NaCl, 20 mM HEPES pH 7.50, and 10 μM **‘8090**. Peak fractions containing the monomeric SERT complex were supplemented with **‘8090** to 30 μM and concentrated to ~10 μM with a 50k MWCO spin filter (Amicon). Monodispersity of the final EM sample was assessed by analytical fluorescence SEC using ~ 5 μg protein and the chromatography buffer and column. Tryptophan fluorescence was recorded with an FP-1520 Intelligent Fluorescence Detector (Jasco) using λex = 280 nm and λem = 350 nm.

The 2.5 μl sample was applied to glow discharged UltrAuFoil (R 1.2/1.3) 300 mesh grids (Qauntifoil). Grids were plunge vitrified into liquid ethane using a Vitrobot Mark IV (Thermo Fisher) with 5 s wait time, 3–5 s blot time, and 0 blot force. The blotting chamber was maintained at 100% humidity and 22°C. Vitrified grids were clipped with Autogrid sample carrier assemblies (Thermo Fisher) immediately prior to imaging.

Movies of **‘8090**-bound MSPNW11-SERT-Fab15B8 embedded in ice were recorded using a Titan Krios Gi3 (Thermo Fisher) equipped with a BioQuantum Energy Filter (Gatan) and a K3 Direct Electron Detector (Gatan). Data were collected using Serial EM [99] running a 3 × 3 image shift script at 0° stage tilt. A 105,000 x nominal magnification with 100 μm objective aperture was used in superresolution mode with a physical pixel size of 0.81 Å pixel^{-1}. Movies were recorded using dose fractionated illumination conditions with a total exposure of 50.0 e^{-} Å^{-2} delivered over 60 frames yielding 0.833 e^{-} Å^{-2} frame^{-1}.

Data processing—Raw movies were imported into cryoSPARC v3.2.0 (Structura Biotechnology), patch motion corrected with 0.5 Fourier cropping, and contrast transfer functions were calculated for the resulting micrographs using Patch CTF Estimation. Particles were template picked using an ab initio model that was generated during data collection in cryoSPARC Live (Structura Biotechnology). A total of 3,313,742 particles were extracted with a 360 pixel box that was binned to 96 pixels, and sorted by two rounds of 3D classification by heterogenous refinement, using initial model templates low pass filtered to 20 Å. Particles were unbinned and subjected to an additional round of sorting by

heterogenous refinement, using two initial models of SERT. Finally non-uniform refinement was performed, before particles were exported using the pyem v0.5 [100]. An inclusion mask covering SERT was generated with the Segger tool in Chimera and the mask.py tool in pyem v0.5. Particles and mask were imported into Relion v3.0 and subjected to 3D classification without image alignment. A series of classifications were performed varying the number of classes and the T factor. The resulting 187,696 particles were brought back into cryoSPARC and non-uniform refinement followed by local refinement using a mask covering SERT and the variable chains of Fab15B8.

A Directional Fourier shell correlation (dFSC) was calculated using half maps and the final output mask from the local refinement [101]. Local resolution estimation were calculated in cryoSPARC. Euler angle distribution was visualized with the star2bild.py script. Model building and refinement were carried out using PDB 6VRH as starting model, which was fit into the 3.0 Å SERT map using ChimeraX [102]. A rough model was generated using ISOLDE extension [103] which was further refined by iterations of real space refinement in Phenix [104] and manual refinement in Coot [105]. The **‘8090** model and rotamer library were generated with PRODRG server [106], and docked using Coot. Final map-model validations were carried out using Molprobity and EMRinger in Phenix.

Behavioral Studies—The learned helplessness, sucrose preference, tail suspension, shock escape, sensitivity to foot-shock, open field, and elevated zero maze apparati and procedures have been described [107]. The equipment and procedures for the elevated plus maze[108] and opioid withdrawal assay [109] have been described. The elevated 8-arm radial maze apparatus has been reported [110]. The mouse was placed into the center zone and given 5 min of free access to the maze. The numbers of arm entries before the first re-entry (i.e., entries to repeat), the numbers of entries before a second repeat, and the total distance traveled are presented.

Drugs and Compounds—All new ligands were synthesized by Enamine (Kyiv, Ukrane) to ≥95% analytic purity. At UCSF **‘8219** was re-suspended in 20% cyclodextran and **‘8090** in NaCl 0.9% for the plus maze and opioid withdrawal assays. Paroxetine hydrochloride and morphine sulfate pentahydrate (Millipore Sigma, St. Louis, MO) were used in the respective plus maze and withdrawal studies where 20% ethanol and saline served as vehicles, respectively. In the Duke behavioral studies, the vehicle consisted of N,N-dimethylacetamide (final volume 0.5%; Millipore Sigma) brought to volume with 5% 2-hydroxypropoyl-β-cyclodextrin (Millipore Sigma) in water (Mediatech Inc., Manassas, VA). As controls, fluoxetine hydrochloride (Flx; Millipore Sigma) and ibogaine (Ibo; NIDA Drug Supply Program, Bethesda, MD) were used. In all experiments, personnel were blinded to the particular treatment and genotype of the mice. All drugs and compounds were administered i.p. at in volumes of either 100 μL (UCSF) or 5 mL/Kg (Duke).

Elevated Plus-Maze Assay—The plus-maze apparatus consisted of two open arms and two closed arms (with 15 cm high, opaque walls) of the same dimensions (35 × 9 cm), elevated to a height of 50 cm. Mice received 100 μL of each compound (10 mg/kg; i.p.) or vehicle (saline for **‘8219**; 20% cyclodextran for **‘8090**) once a day for 10 consecutive days. After the last injection (on the 10th day), mice were placed in a Plexiglas cylinder for 30

min before being placed into the center area of the plus-maze, facing a closed arm. A camera placed ~ 2 m above the maze recorded the amount and the number of times each mouse entered each arm, over a period of 5 min. The total distance travelled in the apparatus was also recorded. A single injection of paroxetine (10 mg/kg. i.p.) was used as positive control. Animals receiving paroxetine were also first habituated for 30 min in a Plexiglas cylinder before entering the plus-maze.

Learned helplessness paradigm and shock escape testing—The learned helplessness (LH) apparatus has been described [81]. C57BL/6J males were housed individually for the entire experiment on a 12:12 light-dark cycle (lights on 0500 h) and were trained/tested in LH between 0900 and 1530 h. One mouse cohort was treated with vehicle, 2 or 5 mg/kg **‘8090**, or 5 mg/kg **‘8219** once a day for 14 days prior to LH training (Figure 6). Chronic administration continued daily during LH training for 21 days and for the first 13 days of LH testing. Subsequently, treatment was withdrawn and the behavioral responses were followed over 10 additional days to determine the duration of the compound/drug effects. A second cohort received vehicle and 10 mg/kg Flx and were treated as described above. Beginning on day 0 the vehicle-treated mice were divided into one group that continued with vehicle, while the other group was given 40 mg/kg Ibo daily over the first 13 days of LH testing and then withdrawn.

For LH training, mice were habituated to the apparatus for 60 min over 2 consecutive days (Figure 6, *top*). During training and testing, all mice were returned to their home-cage with food and water. Next, mice received 360 0.15 mA foot-shocks for 2 s (10 s variable inter-trial interval) on days −19 to −11, −8 to −3, and on −1. On days −14 and −11, mice received foot-shock for the first 30 min, it was stopped for 10 min, and was resumed for the final 20 min. On days −12 and −8, after LH training mice returned to their home-cages without food. On day −10 mice were exposed to a Pulse Ultra Bright LED Strobe Light (Roxant, Bellevue, WA) throughout the dark cycle. On day −9 the bedding, food, and mouse were sprayed with ~8 mL of water and the bedding was not changed for 2 days. On days −9 and −2, mice were tested for shock escape (0.15 mA foot-shock) over 10 trials (inter-trial interval 30–90 s) and the numbers and latencies to escape were determined by MedAssociates software (St. Albans, VT). On days −7 and −6, two-bottle water-water (W-W) training was performed. This was followed on days −5 to −2 with sucrose-water (S-W) pairings.

LH testing began on day 0 and continued through day 23 (Figure 6A, *bottom*). Mice were tested in tail suspension on days 0, 1, 3, 8, 14, 15, 17, and 21. Sucrose-water pairing occurred on days 0, 1, 3, 7, 11, 14, 15, 17, and 21. Shock escape testing was conducted on days 4, 10, 18, and 23. Zero maze testing for anxiety was performed on day 6. On day 9 working memory was evaluated in the 8-arm radial maze. Locomotion was examined on day 12 in the open field. Finally, sensitivity to foot-shock was analyzed on treatment day 13 and treatment-withdrawal on day 22.

Tail suspension—This test was conducted between 1000 and 1500 h with both the VMAT2 and the LH models using the MedAssociates (St. Albans, VT) mouse tail suspension apparatus [81]. Here, the body weight of the mouse was used as a control for the force of struggle activity. In the genetic model, adult (2–4 mos of age) male and female

WT and VMAT2 HET mice were given (i.p.) a single administration of vehicle, 20 mg/kg Flx, 30 mg/kg Ibo, or different doses of **‘8090** or **‘8219**. Thirty min after injection mice were tested for 6 min and at 1, 7, and 12 days post-injection. In the LH model, immobility in tail suspension was assessed at 30 min (day 0) and on days 1, 3, and 8 of treatment and on days 14, 15, 17, and 21 during treatment withdrawal (Figure 6A, *bottom*).

Sucrose preference—This test was conducted in the home-cage with two bottles (Animal Care Systems, Centennial, CO). Water bottles were removed from the home-cage 2.5 h prior to the dark cycle. Mice in the LH study were provided with water-water (W-W) pairings on days −7 and −6 1.5 h after the beginning of the dark cycle with continual access until 0830 h (Figure 6A). Subsequently, on training days −5 to −2 and on testing days 0, 1, 3, 7, 11, 14, 15, 17, and 21, mice were presented with 0.6% sucrose-water (S-W) pairings. The position of the sucrose bottle was alternated over days with the total volume consumed recorded. Sucrose preference was calculated as the volume of sucrose consumed minus that of water, divided by the total volume. Positive values represented a preference for sucrose, negative scores a preference for water, and scores near “0” indicating no preference.

Open field motor activity—In LH mice locomotion was examined in an open field (21 × 21 × 30 cm; Omnitech Electronics, Columbus, OH) illuminated at 180 lux [81]. Animals were placed into the open field for 30 min for baseline activities, were removed, injected with vehicle, **‘8090**, **‘8219**, Ibo, or Flx, and returned immediately to the open field for 30 min (Figure 6A, *bottom*). Locomotion (distance traveled) was monitored using Fusion Integra software (Omnitech) as cumulative activity.

Sensitivity to foot-shock—This test and apparatus have been described [111]. Animals were given vehicle, **‘8090**, **‘8219**, Ibo, or Flx and tested 30 min later during the treatment and treatment-withdrawal phases of LH testing (Figure 6A, *bottom*). Reactivity to foot-shock was evaluated with 0, 0.1, 0.2, and 0.3 mAmp on test days 13 and 22.

Elevated zero maze—The apparatus and procedure are published [81]. Mice were injected with vehicle, **‘8090**, **‘8219**, Ibo, or Flx and tested 30 min later in the zero maze over 5 min on LH test day 6 (Figure 6A, *bottom*). Percent open area time, latency to enter the open areas, and locomotor activities were recorded.

Elevated radial arm maze—The radial maze was made of wood and painted black, it was elevated 45.5 cm from the floor, and each arm was 22 cm long with a central area 11 cm in diameter. From the central zone, the walls of each arm were 7 cm high for 8 cm and the remainder was 2.5 cm high. This test was conducted from 1000–1500 h on day 9 of LH testing (Figure 6A, *bottom*). Mice were administered vehicle, **‘8090**, **‘8219**, Ibo, or Flx and tested 30 min later when placed into the center zone with 5 min of free-access. The numbers of arm entries before the first re-entry (i.e., entries to repeat), numbers of entries before a second repeat, and the total distance traveled are presented

Opioid Withdrawal Assay—The opioid withdrawal assay was conducted as described [109]. Briefly, mice received escalating morphine doses over 4 days (10, 15, 20, 30, 50, 60, 70 and 75 mg/kg; twice daily). On day 5, mice received 20 mg/kg morphine followed 2 h later

by 10 mg/kg **‘8219** or paroxetine, or their vehicles (saline or 20% ethanol, respectively). Thirty min later, all mice received 10 mg/kg naloxone and were filmed over the next 20 min. For withdrawal, we scored over these 20 min the number of naloxone-precipitated jumps, forepaw shakes, wet dog shakes and rearings, as well as the time spent grooming/forepaw licking.

QUANTIFICATION AND STATISTICAL ANALYSIS

All data are presented as means ± standard errors of the mean. UCSF statistical analyses were performed with Prism (GraphPad, San Diego, CA) using unpaired Student’s t-test to compare the effects of the compounds and paroxetine with their vehicle control presented in Figure 7 and supplemental.pdf. At Duke, the data were analyzed by IBM SPSS Statistics 28 programs (IBM, Chicago, IL), the statistical analysis presented in Figures 5, 6, S3, S4, S5 and supplemental.pdf and tables S4–S6. Table S6 provides all the primary statistics for the behavioral studies conducted at Duke, the post-hoc p-values are provided in each panel of the Figures 5, 6, S3, S4, S5 and supplemental.pdf for the behavioral studies, and the Ns (numbers of mice behaviorally tested) are given in Table S6 (Duke) and in the Figure Legends. In the course of performing statistical analyses in the SPSS programs, all statistical outputs from Duke contain Levine’s Test for Equality of Error Variances as a test for homogeneity of variance. Since no sex effects were detected in VMAT2 mice, sex was collapsed in statistical analyses. Student’s t-test, one- or two-way ANOVA, repeated measures ANOVA (RMANOVA), or analysis of covariance (ANCOVA) were followed by Bonferroni corrected pair-wise comparisons. A $p<0.05$ was considered significant. The numbers of animals in each group represent the number of replicates for a given study. The graphic results are presented using GraphPad Prism 9.4.1. Statistical analysis in Figures 2, 3 and supplemental.pdf was performed using Origin (Originlab) where uncertainties and statistical significance of differences were calculated, using 2-sample t-tests and, where possible, paired-sample t-tests. All reported resolutions in cryo-EM studies are based upon the 0.143 Fourier Shell Correlation criterion (Figure 4 and supplemental.pdf).

Supplementary Material

Refer to Web version on PubMed Central for supplementary material.

Acknowledgments:

Supported by DARPA HR0011-19-2-0020 (B.L.R, A.A.B, A.M, & B.K.S), National Institutes of Health R35GM122481 (B.K.S), GM133836 (J.J.I), R01NS102277 (G.R), by the NIMH Psychoactive Drug Screening Program, and the Michael Hooker Distinguished Professorship (B.L.R). We thank the NIDA Drug Supply Program for ibogaine. We thank Dan Toso at Cal-Cryo/QB3-Berkeley for help with microscope operation.

REFERENCES

1. Murphy DL, Fox MA, Timpano KR, Moya PR, Ren-Patterson R, Andrews AM, Holmes A, Lesch KP, and Wendland JR (2008). How the serotonin story is being rewritten by new gene-based discoveries principally related to SLC6A4, the serotonin transporter gene, which functions to influence all cellular serotonin systems. Neuropharmacology 55, 932–960. [PubMed: 18824000]
2. Gu H, Wall SC, and Rudnick G (1994). Stable expression of biogenic amine transporters reveals differences in inhibitor sensitivity, kinetics, and ion dependence. J Biol Chem 269, 7124–7130. [PubMed: 8125921]

3. Jacobs M, Zhang Y, Campbell S, and Rudnick G (2007). Ibogaine, a noncompetitive inhibitor of serotonin transport, acts by stabilizing the cytoplasm-facing state of the transporter. J Biol Chem 282, 29441–29447. [PubMed: 17698848]
4. Bulling S, Schicker K, Zhang Y-W, Stockner T, Gruber C, Boehm S, Freissmuth M, Rudnick G, Sitte HH, and Sandtner W (2012). The mechanistic basis of non-competitive ibogaine inhibition in serotonin and dopamine transporters. Journal of Biological Chemistry 287, 18524–18534. doi: 10.1074/jbc.M112.343681. [PubMed: 22451652]
5. Glick SD, Maisonneuve IM, and Szumlinski KK (2001). Mechanisms of Action of Ibogaine: Relevance to Putative Therapeutic Effects and Development of a Safer Iboga Alkaloid Congener. In Ibogaine: Proceedings of the first International Conference, Alper KR, and Glick SD, eds. (Academic Press), pp. 39–53.
6. Coleman JA, Green EM, and Gouaux E (2016). X-ray structures and mechanism of the human serotonin transporter. Nature 532, 334–339. 10.1038/nature17629. [PubMed: 27049939]
7. Coleman JA, Yang D, Zhao Z, Wen P-C, Yoshioka C, Tajkhorshid E, and Gouaux E (2019). Serotonin transporter–ibogaine complexes illuminate mechanisms of inhibition and transport. Nature 569, 141–145. 10.1038/s41586-019-1135-1. [PubMed: 31019304]
8. Yang D, and Gouaux E (2021). Illumination of serotonin transporter mechanism and role of the allosteric site. Sci Adv 7, eabl3857. 10.1126/sciadv.abl3857. [PubMed: 34851672]
9. Yamashita A, Singh SK, Kawate T, Jin Y, and Gouaux E (2005). Crystal structure of a bacterial homologue of Na^+/Cl^--dependent neurotransmitter transporters. Nature 437, 215–223. 10.1038/nature03978. [PubMed: 16041361]
10. Krishnamurthy H, and Gouaux E (2012). X-ray structures of LeuT in substrate-free outward-open and apo inward-open states. Nature 481, 469–474. 10.1038/nature10737. [PubMed: 22230955]
11. Penmatsa A, Wang KH, and Gouaux E (2013). X-ray structure of dopamine transporter elucidates antidepressant mechanism. Nature 503, 85–90. 10.1038/nature12533. [PubMed: 24037379]
12. Shahsavar A, Stohler P, Bourenkov G, Zimmermann I, Siegrist M, Guba W, Pinard E, Sinning S, Seeger MA, Schneider TR, et al. (2021). Structural insights into the inhibition of glycine reuptake. Nature 591, 677–681. 10.1038/s41586-021-03274-z. [PubMed: 33658720]
13. Gotfryd K, Boesen T, Mortensen JS, Khelashvili G, Quick M, Terry DS, Missel JW, LeVine MV, Gourdon P, Blanchard SC, et al. (2020). X-ray structure of LeuT in an inward-facing occluded conformation reveals mechanism of substrate release. Nat Commun 11, 1005. 10.1038/s41467-020-14735-w. [PubMed: 32081981]
14. Quick M, Yano H, Goldberg NR, Duan L, Beuming T, Shi L, Weinstein H, and Javitch JA (2006). State-dependent conformations of the translocation pathway in the tyrosine transporter Tyt1, a novel neurotransmitter:sodium symporter from Fusobacterium nucleatum. Journal of Biological Chemistry 281, 26444–26454. 10.1074/jbc.M602438200. [PubMed: 16798738]
15. Zhao Y, Terry D, Shi L, Weinstein H, Blanchard SC, and Javitch JA (2010). Single-molecule dynamics of gating in a neurotransmitter transporter homologue. Nature 465, 188–193. 10.1038/nature09057. [PubMed: 20463731]
16. Claxton DP, Quick M, Shi L, de Carvalho FD, Weinstein H, Javitch JA, and Mchaourab HS (2010). Ion/substrate-dependent conformational dynamics of a bacterial homolog of neurotransmitter:sodium symporters. Nature structural & molecular biology 17, 822–829. 10.1038/nsmb.1854.
17. Forrest LR, Zhang YW, Jacobs MT, Gesmonde J, Xie L, Honig BH, and Rudnick G (2008). Mechanism for alternating access in neurotransmitter transporters. Proc Natl Acad Sci U S A 105, 10338–10343. 10.1073/pnas.0804659105. [PubMed: 18647834]
18. Fenollar-Ferrer C, Stockner T, Schwarz TC, Pal A, Gotovina J, Hofmaier T, Jayaraman K, Adhikary S, Kudlacek O, Mehdipour AR, et al. (2014). Structure and regulatory interactions of the cytoplasmic terminal domains of serotonin transporter. Biochemistry 53, 5444–5460. 10.1021/bi500637f. [PubMed: 25093911]
19. Tavoulari S, Margheritis E, Nagarajan A, DeWitt DC, Zhang YW, Rosado E, Ravera S, Rhoades E, Forrest LR, and Rudnick G (2016). Two Na^+ Sites Control Conformational Change in a Neurotransmitter Transporter Homolog. J Biol Chem 291, 1456–1471. 10.1074/jbc.M115.692012. [PubMed: 26582198]

20. Zhang Y-W, Uchendu S, Leone V, Bradshaw RT, Sangwac N, Forrest LR, and Rudnick G (2021). Chloride-dependent conformational changes in the GlyT1 glycine transporter. Proc Natl Acad Sci U S A 118, e2017431118. 10.1073/pnas.2017431118. [PubMed: 33658361]
21. Zhao Y, Terry DS, Shi L, Quick M, Weinstein H, Blanchard SC, and Javitch JA (2011). Substrate-modulated gating dynamics in a Na^+-coupled neurotransmitter transporter homologue. Nature 474, 109–113. 10.1038/nature09971. [PubMed: 21516104]
22. Kazmier K, Sharma S, Quick M, Islam SM, Roux B, Weinstein H, Javitch JA, and McHaourab HS (2014). Conformational dynamics of ligand-dependent alternating access in LeuT. Nature structural & molecular biology 21, 472–479. 10.1038/nsmb.2816.
23. Zhang YW, Turk BE, and Rudnick G (2016). Control of serotonin transporter phosphorylation by conformational state. Proc Natl Acad Sci U S A 113, E2776–E2783. 10.1073/pnas.1603282113. [PubMed: 27140629]
24. Zhang YW, Tavoulari S, Sinning S, Aleksandrova AA, Forrest LR, and Rudnick G (2018). Structural elements required for coupling ion and substrate transport in the neurotransmitter transporter homolog LeuT. Proc Natl Acad Sci U S A 115, E8854–E8862. 10.1073/pnas.1716870115. [PubMed: 30181291]
25. Tavoulari S, Forrest LR, and Rudnick G (2009). Fluoxetine (Prozac) Binding to Serotonin Transporter Is Modulated by Chloride and Conformational Changes. Journal of Neuroscience 29, 9635–9643. 10.1523/jneurosci.0440-09.2009. [PubMed: 19641126]
26. Hasenhuetl PS, Freissmuth M, and Sandtner W (2016). Electrogenic Binding of Intracellular Cations Defines a Kinetic Decision Point in the Transport Cycle of the Human Serotonin Transporter. J Biol Chem 291, 25864–25876. 10.1074/jbc.M116.753319. [PubMed: 27756841]
27. Alper KR, Lotsof HS, Frenken GM, Luciano DJ, and Bastiaans J (1999). Treatment of acute opioid withdrawal with ibogaine. Am J Addict 8, 234–242. [PubMed: 10506904]
28. Brown TK (2013). Ibogaine in the treatment of substance dependence. Current drug abuse reviews 6, 3–16. [PubMed: 23627782]
29. Schenberg EE, de Castro Comis MA, Chaves BR, and da Silveira DX (2014). Treating drug dependence with the aid of ibogaine: a retrospective study. J Psychopharmacol 28, 993–1000. 10.1177/0269881114552713. [PubMed: 25271214]
30. Wasko MJ, Witt-Enderby PA, and Surratt CK (2018). DARK Classics in Chemical Neuroscience: Ibogaine. ACS Chem Neurosci 9, 2475–2483. 10.1021/acschemneuro.8b00294. [PubMed: 30216039]
31. Rodriguez P, Urbanavicius J, Prieto JP, Fabius S, Reyes AL, Havel V, Sames D, Scorza C, and Carrera I (2020). A Single Administration of the Atypical Psychedelic Ibogaine or Its Metabolite Noribogaine Induces an Antidepressant-Like Effect in Rats. ACS Chem Neurosci 10.1021/acschemneuro.0c00152.
32. Wendland JR, DeGuzman TB, McMahon F, Rudnick G, Detera-Wadleigh SD, and Murphy DL (2008). SERT Ileu425Val in autism, Asperger syndrome and obsessive-compulsive disorder. Psychiatr Genet 18, 31–39. 10.1097/YPG.0b013e3282f08a06. [PubMed: 18197083]
33. Zhang YW, Gesmonde J, Ramamoorthy S, and Rudnick G (2007). Serotonin transporter phosphorylation by cGMP-dependent protein kinase is altered by a mutation associated with obsessive compulsive disorder. J Neurosci 27, 10878–10886. 10.1523/jneurosci.0034-07.2007. [PubMed: 17913921]
34. Alon A, Lyu J, Braz JM, Tummino TA, Craik V, O'Meara MJ, Webb CM, Radchenko DS, Moroz YS, Huang XP, et al. (2021). Structures of the σ(2) receptor enable docking for bioactive ligand discovery. Nature 600, 759–764. 10.1038/s41586-021-04175-x. [PubMed: 34880501]
35. Lyu J, Wang S, Balius TE, Singh I, Levit A, Moroz YS, O'Meara MJ, Che T, Algaa E, Tolmachova K, et al. (2019). Ultra-large library docking for discovering new chemotypes. Nature 566, 224–229. 10.1038/s41586-019-0917-9. [PubMed: 30728502]
36. Sadybekov AA, Sadybekov AV, Liu Y, Iliopoulos-Tsoutsouvas C, Huang XP, Pickett J, Houser B, Patel N, Tran NK, Tong F, et al. (2022). Synthon-based ligand discovery in virtual libraries of over 11 billion compounds. Nature 601, 452–459. 10.1038/s41586-021-04220-9. [PubMed: 34912117]

37. Stein RM, Kang HJ, McCorvy JD, Glatfelter GC, Jones AJ, Che T, Slocum S, Huang XP, Savych O, Moroz YS, et al. (2020). Virtual discovery of melatonin receptor ligands to modulate circadian rhythms. Nature 579, 609–614. 10.1038/s41586-020-2027-0. [PubMed: 32040955]
38. Ballante F, Kooistra AJ, Kampen S, de Graaf C, and Carlsson J (2021). Structure-Based Virtual Screening for Ligands of G Protein-Coupled Receptors: What Can Molecular Docking Do for You? Pharmacol Rev 73, 527–565. 10.1124/pharmrev.120.000246. [PubMed: 34907092]
39. Bender BJ, Gahbauer S, Luttens A, Lyu J, Webb CM, Stein RM, Fink EA, Balius TE, Carlsson J, Irwin JJ, and Shoichet BK (2021). A practical guide to large-scale docking. Nat Protoc 16, 4799–4832. 10.1038/s41596-021-00597-z. [PubMed: 34561691]
40. Gabrielsen M, Kurczab R, Ravna AW, Kufareva I, Abagyan R, Chilmonczyk Z, Bojarski AJ, and Sylte I (2012). Molecular mechanism of serotonin transporter inhibition elucidated by a new flexible docking protocol. Eur J Med Chem 47, 24–37. 10.1016/j.ejmech.2011.09.056. [PubMed: 22071255]
41. Gabrielsen M, Wołosewicz K, Zawadzka A, Kossakowski J, Nowak G, Wolak M, Stachowicz K, Siwek A, Ravna AW, Kufareva I, et al. (2013). Synthesis, antidepressant evaluation and docking studies of long-chain alkylnitroquipazines as serotonin transporter inhibitors. Chem Biol Drug Des 81, 695–706. 10.1111/cbdd.12116. [PubMed: 23574807]
42. Gunera J, Baker JG, van Hilten N, Rosenbaum DM, and Kolb P (2020). Structure-Based Discovery of Novel Ligands for the Orexin 2 Receptor. J Med Chem 63, 11045–11053. 10.1021/acs.jmedchem.0c00964. [PubMed: 32977721]
43. Kampen S, Duy Vo D, Zhang X, Panel N, Yang Y, Jaiteh M, Matricon P, Svenningsson P, Brea J, Loza MI, et al. (2021). Structure-Guided Design of G-Protein-Coupled Receptor Polypharmacology. Angew Chem Int Ed Engl 60, 18022–18030. 10.1002/anie.202101478. [PubMed: 33904641]
44. Katritch V, Rueda M, and Abagyan R (2012). Ligand-guided receptor optimization. Methods Mol Biol 857, 189–205. 10.1007/978-1-61779-588-6_8. [PubMed: 22323222]
45. Kolb P, Ferreira RS, Irwin JJ, and Shoichet BK (2009). Docking and chemoinformatic screens for new ligands and targets. Curr Opin Biotechnol 20, 429–436. 10.1016/j.copbio.2009.08.003. [PubMed: 19733475]
46. Kolb P, and Irwin JJ (2009). Docking screens: right for the right reasons? Curr Top Med Chem 9, 755–770. 10.2174/156802609789207091. [PubMed: 19754393]
47. Kufareva I, Chen YC, Ilatovskiy AV, and Abagyan R (2012). Compound activity prediction using models of binding pockets or ligand properties in 3D. Curr Top Med Chem 12, 1869–1882. 10.2174/156802612804547335. [PubMed: 23116466]
48. Kufareva I, Gustavsson M, Zheng Y, Stephens BS, and Handel TM (2017). What Do Structures Tell Us About Chemokine Receptor Function and Antagonism? Annu Rev Biophys 46, 175–198. 10.1146/annurev-biophys-051013-022942. [PubMed: 28532213]
49. Kufareva I, Stephens BS, Holden LG, Qin L, Zhao C, Kawamura T, Abagyan R, and Handel TM (2014). Stoichiometry and geometry of the CXC chemokine receptor 4 complex with CXC ligand 12: molecular modeling and experimental validation. Proc Natl Acad Sci U S A 111, E5363–5372. 10.1073/pnas.1417037111. [PubMed: 25468967]
50. Manglik A, Lin H, Aryal DK, McCorvy JD, Dengler D, Corder G, Levit A, Kling RC, Bernat V, Hübner H, et al. (2016). Structure-based discovery of opioid analgesics with reduced side effects. Nature 537, 185–190. 10.1038/nature19112. [PubMed: 27533032]
51. Ngo T, Kufareva I, Coleman J, Graham RM, Abagyan R, and Smith NJ (2016). Identifying ligands at orphan GPCRs: current status using structure-based approaches. Br J Pharmacol 173, 2934–2951. 10.1111/bph.13452. [PubMed: 26837045]
52. Orry AJ, Abagyan RA, and Cavasotto CN (2006). Structure-based development of target-specific compound libraries. Drug Discov Today 11, 261–266. 10.1016/s1359-6446(05)03717-7. [PubMed: 16580603]
53. Ortiz Zacarías NV, Chahal KK, Šimková T, van der Horst C, Zheng Y, Inoue A, Theunissen E, Mallee L, van der Es D, Louvel J, et al. (2021). Design and Characterization of an Intracellular Covalent Ligand for CC Chemokine Receptor 2. J Med Chem 64, 2608–2621. 10.1021/acs.jmedchem.0c01137. [PubMed: 33600174]

54. Patel N, Huang XP, Grandner JM, Johansson LC, Stauch B, McCorvy JD, Liu Y, Roth B, and Katritch V (2020). Structure-based discovery of potent and selective melatonin receptor agonists. Elife 9. 10.7554/eLife.53779.
55. Rognan D (2012). Fragment-based approaches and computer-aided drug discovery. Top Curr Chem 317, 201–222. 10.1007/128_2011_182. [PubMed: 21710380]
56. Rognan D (2017). The impact of in silico screening in the discovery of novel and safer drug candidates. Pharmacol Ther 175, 47–66. 10.1016/j.pharmthera.2017.02.034. [PubMed: 28223231]
57. Roth BL, Irwin JJ, and Shoichet BK (2017). Discovery of new GPCR ligands to illuminate new biology. Nat Chem Biol 13, 1143–1151. 10.1038/nchembio.2490. [PubMed: 29045379]
58. Sadybekov AA, Brouillette RL, Marin E, Sadybekov AV, Luginina A, Gusach A, Mishin A, Besserer-Offroy É, Longpré JM, Borshchevskiy V, et al. (2020). Structure-Based Virtual Screening of Ultra-Large Library Yields Potent Antagonists for a Lipid GPCR. Biomolecules 10. 10.3390/biom10121634.
59. Scharf MM, Bünemann M, Baker JG, and Kolb P (2019). Comparative Docking to Distinct G Protein-Coupled Receptor Conformations Exclusively Yields Ligands with Agonist Efficacy. Mol Pharmacol 96, 851–861. 10.1124/mol.119.117515. [PubMed: 31624135]
60. Stauch B, Johansson LC, McCorvy JD, Patel N, Han GW, Huang XP, Gati C, Batyuk A, Slocum ST, Ishchenko A, et al. (2019). Structural basis of ligand recognition at the human MT(1) melatonin receptor. Nature 569, 284–288. 10.1038/s41586-019-1141-3. [PubMed: 31019306]
61. Uprety R, Che T, Zaidi SA, Grinnell SG, Varga BR, Faouzi A, Slocum ST, Allaoa A, Varadi A, Nelson M, et al. (2021). Controlling opioid receptor functional selectivity by targeting distinct subpockets of the orthosteric site. Elife 10. 10.7554/eLife.56519.
62. Weiss DR, Ahn S, Sassano MF, Kleist A, Zhu X, Strachan R, Roth BL, Lefkowitz RJ, and Shoichet BK (2013). Conformation guides molecular efficacy in docking screens of activated β−2 adrenergic G protein coupled receptor. ACS Chem Biol 8, 1018–1026. 10.1021/cb400103f. [PubMed: 23485065]
63. Wisler JW, Rockman HA, and Lefkowitz RJ (2018). Biased G Protein-Coupled Receptor Signaling: Changing the Paradigm of Drug Discovery. Circulation 137, 2315–2317. 10.1161/circulationaha.117.028194. [PubMed: 29844068]
64. Rudnick G (1977). Active transport of 5-hydroxytryptamine by plasma membrane vesicles isolated from human blood platelets. J Biol Chem 252, 2170–2174. [PubMed: 849926]
65. Kantcheva AK, Quick M, Shi L, Winther A-ML, Stolzenberg S, Weinstein H, Javitch JA, and Nissen P (2013). Chloride binding site of neurotransmitter sodium symporters. Proceedings of the National Academy of Sciences 110, 8489–8494. 10.1073/pnas.1221279110.
66. Tatsumi M, Groshan K, Blakely RD, and Richelson E (1997). Pharmacological profile of antidepressants and related compounds at human monoamine transporters. Eur J Pharmacol 340, 249–258. 10.1016/s0014-2999(97)01393-9. [PubMed: 9537821]
67. Mysinger MM, Weiss DR, Ziarek JJ, Gravel S, Doak AK, Karpiak J, Heveker N, Shoichet BK, and Volkman BF (2012). Structure-based ligand discovery for the protein-protein interface of chemokine receptor CXCR4. Proc Natl Acad Sci U S A 109, 5517–5522. 10.1073/pnas.1120431109. [PubMed: 22431600]
68. Oprea TI (2002). Virtual Screening in Lead Discovery: A Viewpoint. Molecules 7, 51–62. 10.3390/70100051.
69. Irwin JJ, Tang KG, Young J, Dandarchuluun C, Wong BR, Khurelbaatar M, Moroz YS, Mayfield J, and Sayle RA (2020). ZINC20—A Free Ultralarge-Scale Chemical Database for Ligand Discovery. Journal of Chemical Information and Modeling 60, 6065–6073. 10.1021/acs.jcim.0c00675. [PubMed: 33118813]
70. Gu S, Smith MS, Yang Y, Irwin JJ, and Shoichet BK (2021). Ligand Strain Energy in Large Library Docking. J Chem Inf Model 61, 4331–4341. 10.1021/acs.jcim.1c00368. [PubMed: 34467754]
71. Gaulton A, Hersey A, Nowotka M, Bento AP, Chambers J, Mendez D, Mutowo P, Atkinson F, Bellis LJ, Cibrián-Uhalte E, et al. (2017). The ChEMBL database in 2017. Nucleic Acids Res 45, D945–d954. 10.1093/nar/gkw1074. [PubMed: 27899562]

72. Pettersen EF, Goddard TD, Huang CC, Couch GS, Greenblatt DM, Meng EC, and Ferrin TE (2004). UCSF Chimera--a visualization system for exploratory research and analysis. J Comput Chem 25, 1605–1612. 10.1002/jcc.20084. [PubMed: 15264254]
73. Rudnick G, and Wall SC (1992). The molecular mechanism of "ecstasy" [3,4-methylenedioxy-methamphetamine (MDMA)]: serotonin transporters are targets for MDMA-induced serotonin release. Proc Natl Acad Sci U S A 89, 1817–1821. [PubMed: 1347426]
74. Wall SC, Gu H, and Rudnick G (1995). Biogenic amine flux mediated by cloned transporters stably expressed in cultured cell lines: amphetamine specificity for inhibition and efflux. Mol Pharmacol 47, 544–550. [PubMed: 7700252]
75. Jacobs MT, Zhang Y-W, Campbell SD, and Rudnick G (2007). Ibogaine, a Noncompetitive Inhibitor of Serotonin Transport, Acts by Stabilizing the Cytoplasm-facing State of the Transporter. J. Biol. Chem 282, 29441–29447. 10.1074/jbc.M704456200. [PubMed: 17698848]
76. Nasr ML, Baptista D, Strauss M, Sun ZJ, Grigoriu S, Huser S, Plückthun A, Hagn F, Walz T, Hogle JM, and Wagner G (2017). Covalently circularized nanodiscs for studying membrane proteins and viral entry. Nat Methods 14, 49–52. 10.1038/nmeth.4079. [PubMed: 27869813]
77. Kroeze WK, Sassano MF, Huang XP, Lansu K, McCorvy JD, Giguère PM, Sciaky N, and Roth BL (2015). PRESTO-Tango as an open-source resource for interrogation of the druggable human GPCRome. Nature structural & molecular biology 22, 362–369. 10.1038/nsmb.3014.
78. Freis ED (1954). Mental depression in hypertensive patients treated for long periods with large doses of reserpine. N Engl J Med 251, 1006–1008. 10.1056/nejm195412162512504. [PubMed: 13214379]
79. Maes M, Meltzer HY, Cosyns P, and Schotte C (1994). Evidence for the existence of major depression with and without anxiety features. Psychopathology 27, 1–13. 10.1159/000284842. [PubMed: 7972633]
80. Schildkraut JJ (1965). The catecholamine hypothesis of affective disorders: a review of supporting evidence. Am J Psychiatry 122, 509–522. 10.1176/ajp.122.5.509. [PubMed: 5319766]
81. Fukui M, Rodriguiz RM, Zhou J, Jiang SX, Phillips LE, Caron MG, and Wetsel WC (2007). *Vmat2* heterozygous mutant mice display a depressive-like phenotype. J Neurosci 27, 10520–10529. 10.1523/jneurosci.4388-06.2007. [PubMed: 17898223]
82. Price RB, and Duman R (2020). Neuroplasticity in cognitive and psychological mechanisms of depression: an integrative model. Mol Psychiatry 25, 530–543. 10.1038/s41380-019-0615-x. [PubMed: 31801966]
83. Gray AM (2002). The effect of fluvoxamine and sertraline on the opioid withdrawal syndrome: a combined in vivo cerebral microdialysis and behavioural study. Eur Neuropsychopharmacol 12, 245–254. 10.1016/s0924-977x(02)00028-7. [PubMed: 12007676]
84. Rafieian-Kopaei M, Gray AM, Spencer PS, and Sewell RD (1995). Contrasting actions of acute or chronic paroxetine and fluvoxamine on morphine withdrawal-induced place conditioning. Eur J Pharmacol 275, 185–189. 10.1016/0014-2999(94)00770-8. [PubMed: 7796854]
85. Bröer S.a.R., G. (2019). SLC6 neurotransmitter transporter family (version 2019.4) in the IUPHAR/BPS Guide to Pharmacology Database. IUPHAR/BPS Guide to Pharmacology version 2019 4.
86. Southan C, Sharman JL, Benson HE, Faccenda E, Pawson AJ, Alexander SP, Buneman OP, Davenport AP, McGrath JC, Peters JA, et al. (2016). The IUPHAR/BPS Guide to PHARMACOLOGY in 2016: towards curated quantitative interactions between 1300 protein targets and 6000 ligands. Nucleic Acids Res 44, D1054–1068. 10.1093/nar/gkv1037. [PubMed: 26464438]
87. Coleman RG, Carchia M, Sterling T, Irwin JJ, and Shoichet BK (2013). Ligand pose and orientational sampling in molecular docking. PLoS One 8, e75992. 10.1371/journal.pone.0075992. [PubMed: 24098414]
88. Mysinger MM, and Shoichet BK (2010). Rapid context-dependent ligand desolvation in molecular docking. J Chem Inf Model 50, 1561–1573. 10.1021/ci100214a. [PubMed: 20735049]
89. Wei BQ, Baase WA, Weaver LH, Matthews BW, and Shoichet BK (2002). A model binding site for testing scoring functions in molecular docking. J Mol Biol 322, 339–355. 10.1016/s0022-2836(02)00777-5. [PubMed: 12217695]

90. Word JM, Lovell SC, Richardson JS, and Richardson DC (1999). Asparagine and glutamine: using hydrogen atom contacts in the choice of side-chain amide orientation. J Mol Biol 285, 1735–1747. 10.1006/jmbi.1998.2401. [PubMed: 9917408]

91. Case DA et al. (2015). AMBER 2015

92. Gallagher K, and Sharp K (1998). Electrostatic contributions to heat capacity changes of DNA-ligand binding. Biophys J 75, 769–776. 10.1016/s0006-3495(98)77566-6. [PubMed: 9675178]

93. Sharp KA (1995). Polyelectrolyte electrostatics: Salt dependence, entropic, and enthalpic contributions to free energy in the nonlinear Poisson–Boltzmann model. Biopolymers 36, 227–243.

94. Meng EC, Shoichet BK & Kuntz ID (1992). Automated docking with grid-based energy evaluation. J. Comput. Chem 13, 505–524.

95. Zhang YW, and Rudnick G (2005). Cysteine scanning mutagenesis of serotonin transporter intracellular loop 2 suggests an alpha-helical conformation. J Biol Chem 280, 30807–30813. [PubMed: 15994310]

96. Zhang YW, and Rudnick G (2006). The cytoplasmic substrate permeation pathway of serotonin transporter. J Biol Chem 281, 36213–36220. 10.1074/jbc.M605468200. [PubMed: 17008313]

97. Schicker K, Uzelac Z, Gesmonde J, Bulling S, Stockner T, Freissmuth M, Boehm S, Rudnick G, Sitte HH, and Sandtner W (2012). A unifying concept of serotonin transporter associated currents. Journal of Biological Chemistry 287, 438–445. 10.1074/jbc.M111.304261. [PubMed: 22072712]

98. Billesbølle CB, Azumaya CM, Kretsch RC, Powers AS, Gonen S, Schneider S, Arvedson T, Dror RO, Cheng Y, and Manglik A (2020). Structure of hepcidin-bound ferroportin reveals iron homeostatic mechanisms. Nature 586, 807–811. 10.1038/s41586-020-2668-z. [PubMed: 32814342]

99. Mastronarde DN (2003). SerialEM: A Program for Automated Tilt Series Acquisition on Tecnai Microscopes Using Prediction of Specimen Position. Microscopy and Microanalysis 9, 1182–1183. 10.1017/S1431927603445911.

100. Asarnow D, Palovcak E, Cheng Y (2019). asarnow/pyem: UCSF pyem v0.5

101. Dang S, Feng S, Tien J, Peters CJ, Bulkley D, Lolicato M, Zhao J, Zuberbühler K, Ye W, Qi L, et al. (2017). Cryo-EM structures of the TMEM16A calcium-activated chloride channel. Nature 552, 426–429. 10.1038/nature25024. [PubMed: 29236684]

102. Goddard TD, Huang CC, Meng EC, Pettersen EF, Couch GS, Morris JH, and Ferrin TE (2018). UCSF ChimeraX: Meeting modern challenges in visualization and analysis. Protein Sci 27, 14–25. 10.1002/pro.3235. [PubMed: 28710774]

103. Croll TI (2018). ISOLDE: a physically realistic environment for model building into low-resolution electron-density maps. Acta Crystallogr D Struct Biol 74, 519–530. 10.1107/s2059798318002425. [PubMed: 29872003]

104. Adams PD, Afonine PV, Bunkóczi G, Chen VB, Davis IW, Echols N, Headd JJ, Hung LW, Kapral GJ, Grosse-Kunstleve RW, et al. (2010). PHENIX: a comprehensive Python-based system for macromolecular structure solution. Acta Crystallogr D Biol Crystallogr 66, 213–221. 10.1107/s0907444909052925. [PubMed: 20124702]

105. Emsley P, and Cowtan K (2004). Coot: model-building tools for molecular graphics. Acta Crystallogr D Biol Crystallogr 60, 2126–2132. 10.1107/s0907444904019158. [PubMed: 15572765]

106. Schüttelkopf AW, and van Aalten DM (2004). PRODRG: a tool for high-throughput crystallography of protein-ligand complexes. Acta Crystallogr D Biol Crystallogr 60, 1355–1363. 10.1107/s0907444904011679. [PubMed: 15272157]

107. Kaplan AL, Confair DN, Kim K, Barros-Álvarez X, Rodriguiz RM, Yang Y, Kweon OS, Che T, McCorvy JD, Kamber DN, et al. (2022). Bespoke library docking for 5-HT(2A) receptor agonists with antidepressant activity. Nature 610, 582–591. 10.1038/s41586-022-05258-z. [PubMed: 36171289]

108. Urban R, Scherrer G, Goulding EH, Tecott LH, and Basbaum AI (2011). Behavioral indices of ongoing pain are largely unchanged in male mice with tissue or nerve injury-induced mechanical hypersensitivity. Pain 152, 990–1000. 10.1016/j.pain.2010.12.003. [PubMed: 21256675]

109. Wilson LL, Chakraborty S, Eans SO, Cirino TJ, Stacy HM, Simons CA, Uprety R, Majumdar S, and McLaughlin JP (2021). Kratom Alkaloids, Natural and Semi-Synthetic, Show Less Physical Dependence and Ameliorate Opioid Withdrawal. Cell Mol Neurobiol 41, 1131–1143. 10.1007/s10571-020-01034-7. [PubMed: 33433723]

110. Gainetdinov RR, Wetsel WC, Jones SR, Levin ED, Jaber M, and Caron MG (1999). Role of serotonin in the paradoxical calming effect of psychostimulants on hyperactivity. Science 283, 397–401. 10.1126/science.283.5400.397. [PubMed: 9888856]

111. Wetsel WC, Rodriguiz RM, Guillemot J, Rousselet E, Essalmani R, Kim IH, Bryant JC, Marcinkiewicz J, Desjardins R, Day R, et al. (2013). Disruption of the expression of the proprotein convertase PC7 reduces BDNF production and affects learning and memory in mice. Proc Natl Acad Sci U S A 110, 17362–17367. 10.1073/pnas.1314698110. [PubMed: 24101515]

112. Wang YM, Gainetdinov RR, Fumagalli F, Xu F, Jones SR, Bock CB, Miller GW, Wightman RM, and Caron MG (1997). Knockout of the vesicular monoamine transporter 2 gene results in neonatal death and supersensitivity to cocaine and amphetamine. Neuron 19, 1285–1296. 10.1016/s0896-6273(00)80419-5. [PubMed: 9427251]

113. Zivanov J, Nakane T, Forsberg BO, Kimanius D, Hagen WJ, Lindahl E, and Scheres SH (2018). New tools for automated high-resolution cryo-EM structure determination in RELION-3. Elife 7. 10.7554/eLife.42166.

Highlights

- Large library docking finds conformationally- and target-selective SERT inhibitors.
- Cryo-EM supports the computationally-predicted structure.
- The inhibitors are anti-depressant-like and alleviate opioid withdrawal in mice.
- Targeting of transporters for structure-based ligand discovery.

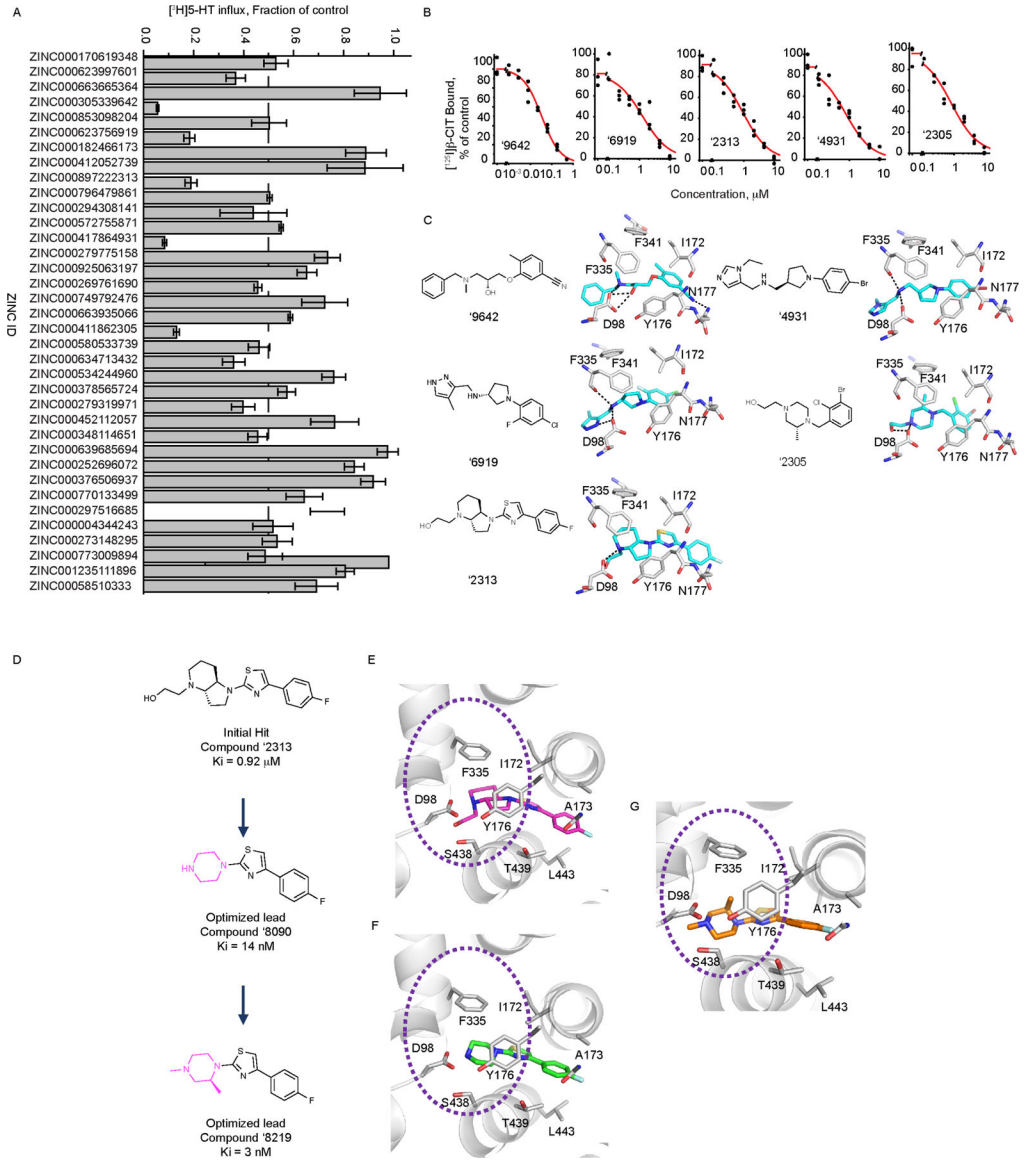

Figure 1. Docking-derived inhibitors of serotonin transporter.

(**A**) Inhibition of [^{3}H]5-HT transport by docking-derived molecules, tested at 30 μM (Table S1). (**B**) Radio-ligand displacement of the top five docking hits (representative curves; summary data in Table S2). (**C**) 2D Chemical structures of the top five docking hits and their docked poses. Interactions are depicted as black dashed lines, ligand carbons in cyan and protein carbons in grey. Oxygens for both protein and ligand are red, nitrogen blue, and sulfur yellow. (**D**) Chemical structures of the parent compound, **'2313** and its optimized analogs **'8090** (Ki 14 nM) and **'8219** (Ki 3 nM). The variable group in the analogs versus the parent are colored in magenta. Comparing the docked poses of (**E**) the parent **'2313** (**F**) **'8090** and (**G**) **'8219**. Dashed circles represent modeled improved stacking of F335 with ring substitutions in going from parent to the optimized analogs.

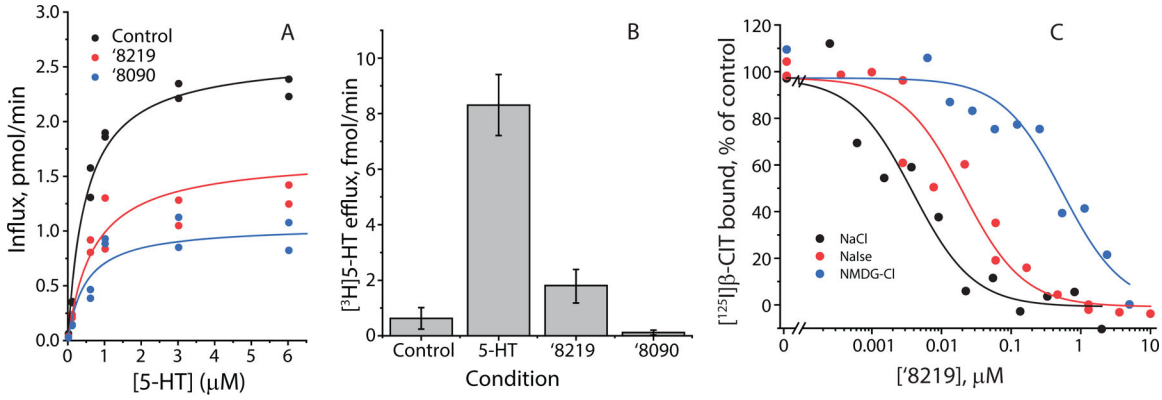

Figure 2.

(A) Kinetics of inhibition by 0.15 μM '8219 and 0.7 μM '8090 (representative experiment). 5-HT transport into HeLa cells transfected with rSERT was non-competitively inhibited by both compounds. There was a small but statistically insignificant increase in KM with '8219 (0.69 ± 0.25 μM (SEM), n=6) and a decrease with '8090 (0.47 ± 0.05 μM, n=5) compared with uninhibited control (0.59 ± 0.18 μM, n=8). P values for paired t-tests were 0.99 and 0.18, respectively. Vmax was significantly decreased for both compounds from 1.7 ± 0.25 pmol/m/well for control (n=8) to 1.1 ± 0.2 pmol/m/well (n=6) for '8219 and 0.69 ± 0.1 pmol/m/well (n=5) for '8090. P values for paired t-tests were 0.018 and 0.011, respectively. **(B)** Efflux of accumulated [3H]5-HT induced by extracellular unlabeled 20 μM 5-HT, 10 μM '8219 or 10 μM '8090. 5-HT induced marked efflux of radiolabel, 8.3 ± 1.1 fmol/m (SEM)(n=6), relative to control (no addition) 0.63 ± 0.39 fmol/m (P=7×10–4 in 2-sample t-test, n=6). '8219 slightly increased efflux (1.8±0.6 fmol/m (SEM) but the increase was not significant (P=0.18, n=6) and '8090 barely increased efflux (0.12±0.09 fmol/m (SEM) (P=0.25, n=5). **(C)** Na+ and Cl− increased '8219 affinity in equilibrium displacement of [125I]β-CIT (representative experiment). Membranes from cells expressing SERT were incubated with 0.1 nM [125I]β-CIT and the indicated concentrations of '8219 in PBS/CM (control, blue line and circles), PBS/CM in which Na+ was replaced with NMDG+ (black line and circles) or Cl− was replaced with isethionate (red line and circles). The presence of Cl− increased '8219 inhibitory potency over 4-fold, from a KI of 21 ± 3 nM to 4.8 ± 1.0 nM (SEM) (n=4, P=0.001). Na+ increased '8219 inhibitory potency 131-fold, from a KI of 527 ± 143 nM to 4.0 ± 0.4 nM (SEM) (n=4, P=0.004).

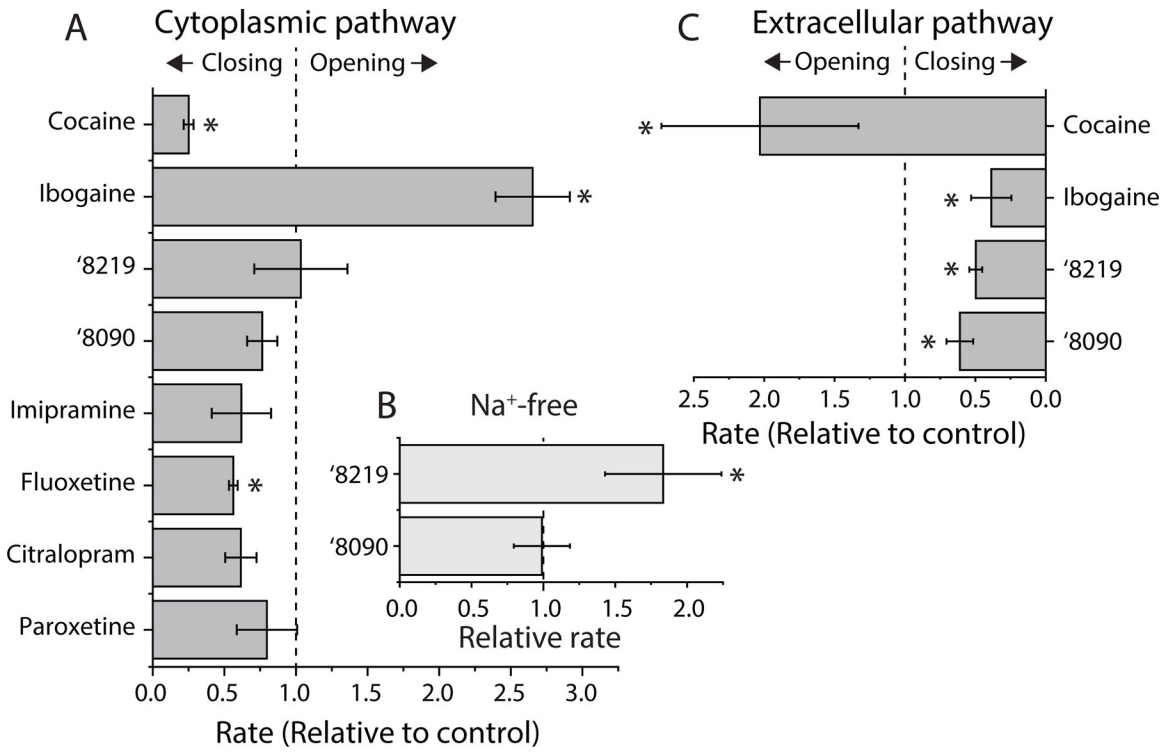

Figure 3. Influence of '8219, '8090 and ibogaine on SERT conformation.

(A) Effects on Cys277 reactivity in the cytoplasmic pathway. Rates of Cys277 modification in membranes from HeLa cells expressing SERT-S277C by MTSEA was measured by the decrease in β-CIT binding activity after treatment with MTSEA in the presence of the indicated compounds (cocaine, 10 μM, n=7; ibogaine, 10 μM, n=10; '8219, 0.05 μM, n=3; '8090 0.15 μM, n=4; imipramine, 0.6 μM, n=3; fluoxetine, 0.13 μM, n=3; citalopram, 0.03 μM, n=3; paroxetine, 0.02 μM, n=3). The reference compounds cocaine and ibogaine are shown at the top, and several clinically used antidepressants are shown at the bottom of the plot. Between them are **'8219** and **'8090**. The control rate was 75 ± 15 $s^{-1}M^{-1}$ (n=18) and error bars represent SEM. **(B)** Effects on Cys277 reactivity in the absence of Na^+ (replaced by NMDG). Rates were measured as above for control (n=6), **'8219** (2 μM, n=6) and **'8090** (2 μM, n=5). The control rate was 26 ± 5 $s^{-1}M^{-1}$ and the error bars represent SEM. **'8219** significantly (P=0.04) increased the rate relative to control. **(C)** Effects on Cys107 reactivity in the extracellular pathway. Rates of Cys107 modification in HeLa cells expressing SERT-Y107C was measured by the decrease in residual transport activity after treatment with MTSET in the presence of the indicated compounds, each present at a saturating concentration (10x KD). Rates were measured as above for control (n=8), cocaine (n=3), ibogaine (n=4), '8219 (n=7) and '8090 (n=4). The control rate was 122 ± 14 $s^{-1}M^{-1}$. *=P<0.05 (paired t-test).

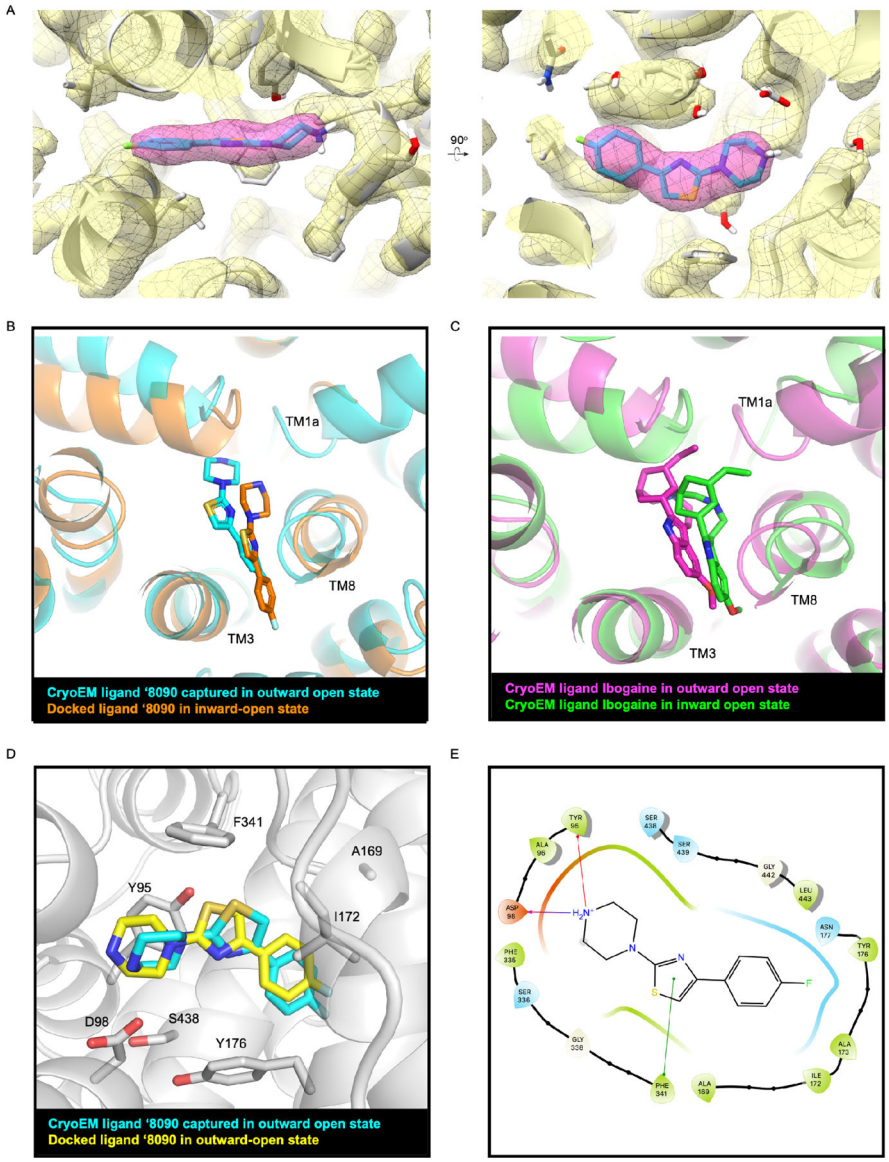

Figure 4. Structural fidelity between the docked and cryo-EM poses of '8090.

(**A**) Cryo-EM density maps of '**8090** bound to SERT in the outward-open state (PDB: 7TXT, EMBD: EMD-26160. (**B**) Comparison of **'8090**'s pose in cryo-EM structure (cyan) and the predicted docked pose in the inward open state of SERT (orange). (**C**) Comparison of ibogaine's pose in cryo-EM determined inward open state structure (green, PDB ID: 6DZZ) and outward open state of structure of SERT (magenta, PDB ID: 6DZY). (**D**) Ligand cryo-EM determined pose (cyan) overlaid with the docked pose (yellow) in the outward open active site of SERT. (**E**) 2D outline of protein−ligand interactions between **'8090** and SERT.

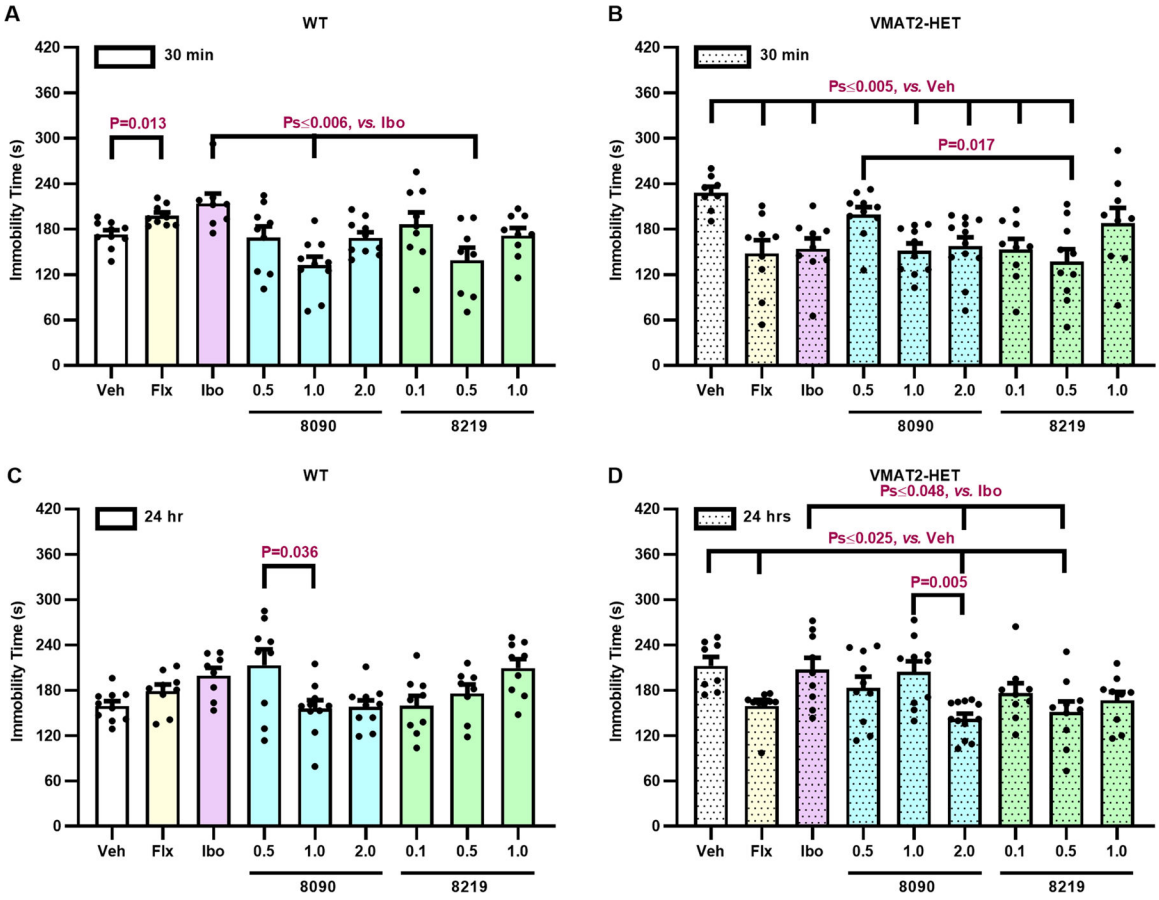

Figure 5. Anti-depressive-like effects of compounds 8090 and 8219 in the tail suspension test with *Vmat2* mice.

*(***A-B**) Acute effects of '**8090** (0.5, 1, and 2 mg/kg) and '**8219** (0.1, 0.5, and 1 mg/kg) 30 min after injection in wild-type (WT) and VMAT2 heterozygous (HET) mice. Controls were given the vehicle (Veh), 20 mg/kg fluoxetine (Flx), or 30 mg/kg ibogaine (Ibo). (**C-D**) Persistent effects of '**8090** and '**8219** 1 day post-injection in WT and VMAT2 HET mice. N=8–10 mice/genotype/treatment. All primary statistics are found in Table S9.

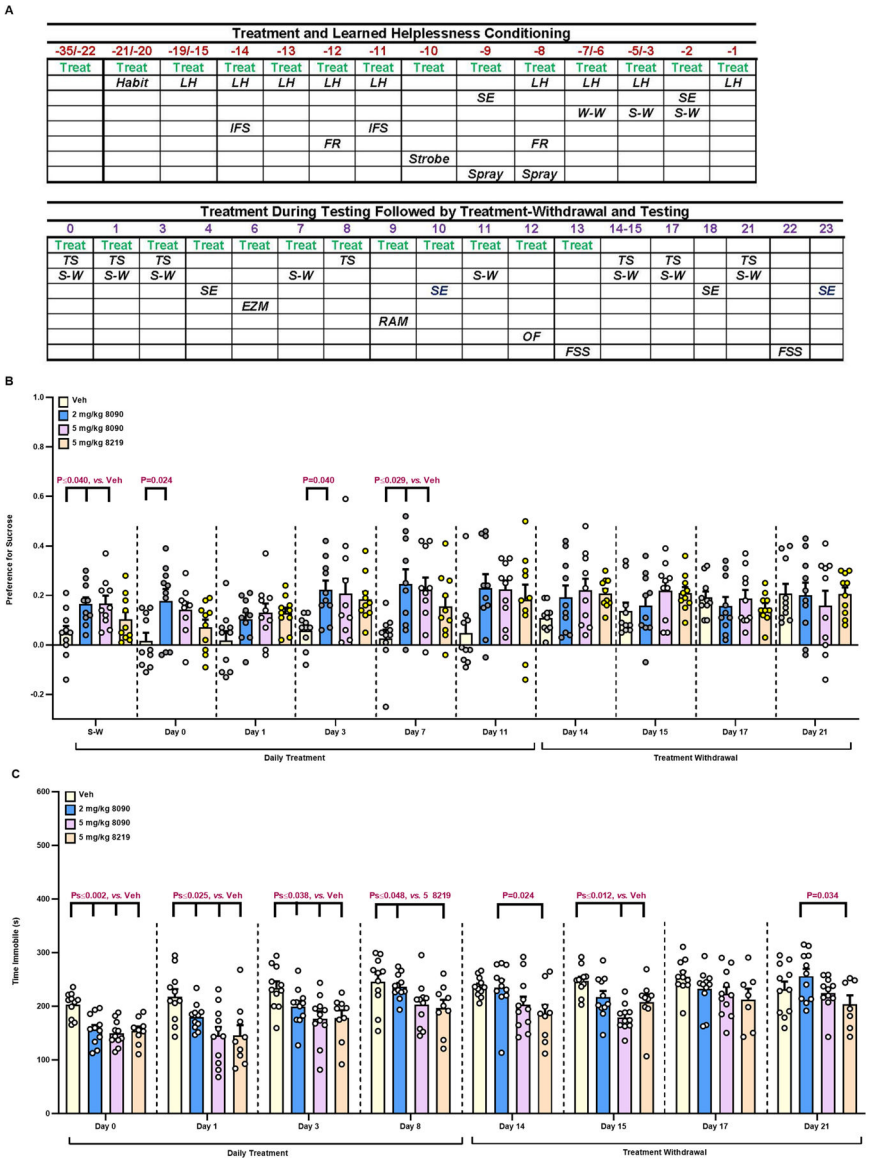

Figure 6. The learned helplessness experimental design with sucrose preference and tail suspension using C57BL/6J mice.

(**A**) *Top:* Sub-chronic administration with the vehicle, 2 or 5 mg/kg **‘8090**, or 5 mg/kg **‘8219** for 2 weeks followed immediately by chronic daily treatment throughout learned helplessness (LH) training. *Bottom:* Continued daily injections during the first 13 days of LH testing, followed by the withdrawal of treatment during testing. Abbreviations: Treat, treatment; Habit, habituation to the LH apparatus; LH, LH training; SE, shock escape testing; W-W, water-water pairing; S-W, sucrose-water pairing; IFS, intermittent foot-shock; FR, overnight food restriction; Strobe, strobe light during the dark cycle; Spray, the mouse and bedding were sprayed with water and the bedding was changed 2-days later; TS, tail suspension; EZM, elevated zero maze; RAM, radial 8-arm maze; OF, open field; and FSS, foot-shock sensitivity. (**B**) Sucrose preference in LH mice. N=10 mice/treatment. (**C**) Tail suspension in LH mice. N=10 mice/treatment. All primary statistics are in Table S9.

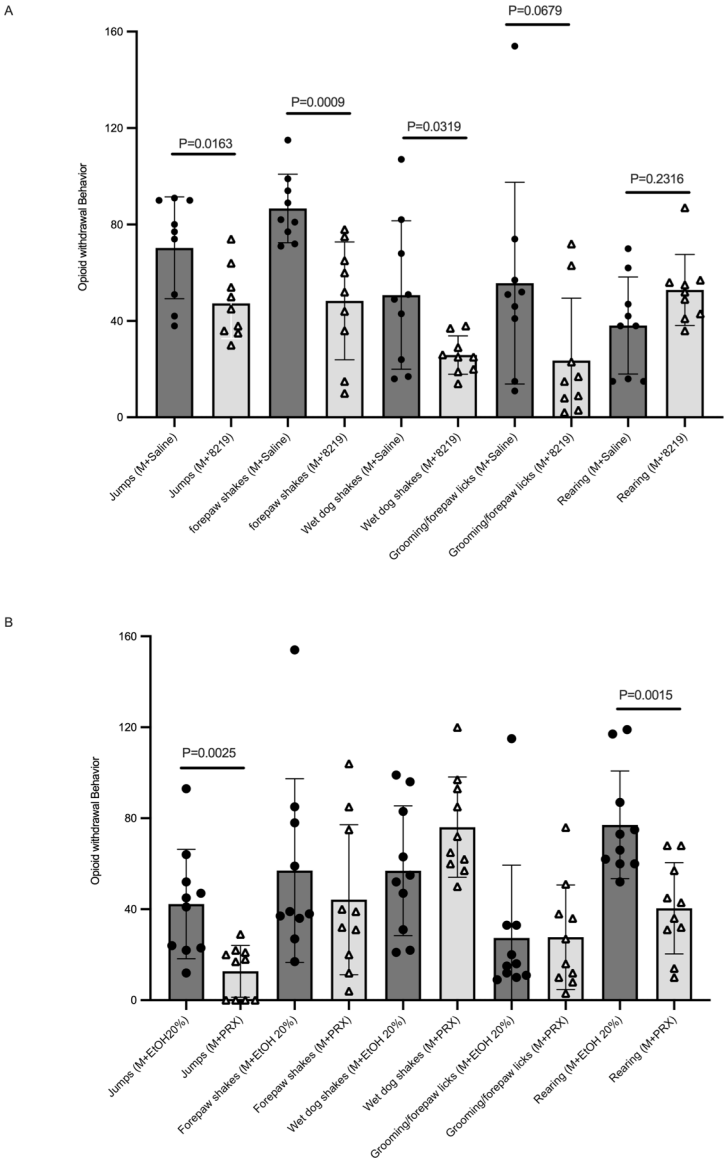

Figure 7: The new SERT inhibitor ‘8219 reduces opioid withdrawal symptoms.

(**A**) Effect of systemic **‘8219** (10 mg/kg; N=9) on naloxone-precipitated morphine (M) withdrawal. (**B**) Effect of systemic paroxetine (PRX; 10 mg/kg; N=9) on withdrawal. Data are presented as means ± SEM with unpaired Student’s t-tests comparing effects of **‘8219** and paroxetine to saline and 20% ethanol, respectively.

Key resources table

REAGENT or RESOURCE	SOURCE	IDENTIFIER
Bacterial and virus strains		
E. coli: XL1-Blue	QB3 Macrolab, UC Berkeley	N/A
E. coli: Rosetta2 (DE3) pLysS	QB3 Macrolab, UC Berkeley	N/A
Chemicals, peptides, and recombinant proteins		
DDM: n-Dodecyl-β-D-Maltoside	Anatrace	Cat# D310
CHS: Cholesteryl Hemisuccinate Tris Salt	Anatrace	Cat# CH210
Protein C peptide: EDQVDPRLIDGK	Genscript	N/A
POPC: 1-palmitoyl-2-oleoyl-glycero-3-phosphocholine	Avanti Polar Lipids	Cat# 850457
POPG: 1-palmitoyl-2-oleoyl-sn-glycero-3-phospho-(1'-rac-glycerol) (sodium salt)	Avanti Polar Lipids	Cat# 840457
Bio-Beads SM-2 Adsorbents	BioRad	Cat# 1523920
HisPur Ni-NTA Resin	Thermo Fisher Scientific	Cat# 88223
Ibogaine hydrochloride	NIDA Drug Supply Program	NIDA # 7260-001
Fluoxetine hydrochloride	Millipore Sigma	F132
N,N-dimethylacetamide	Millipore Sigma	ARK-2190
2-Hydroxypropoyl-β-cyclodextrin	Millipore Sigma/TCI	778966/H0979
Sterile water	Corning (MediaTech)	46-000-Cl
Sucrose (Quick Dissolve Superfine Pure Cane)	Domino	411096
Critical commercial assays		
Q5 High-Fidelity 2X Master Mix	New England Bio-Labs	Cat# M0492
NucleoBond Xtra Midi Plus kit	Macherey-Nagel	Cat# 740412.50
ExpiFectamine 293 Transfection Kit	Thermo Fisher Scientific	Cat# A14524
Deposited data		
Coordinates: SERT-Fab15B8 '8090-bound	This paper	PDB: 7TXT
Experimental models: Cell lines		
Human: Expi293F Inducible Cells	Thermo Fisher Scientific	Cat# A39241
Experimental models: Organisms/strains		
Vesicular monoamine transporter 2 mice	Wang et al., 1997	N/A
C57BL/6J mice	The Jackson Laboratories	JAX: 000664
Oligonucleotides		
Primer: SERT Forward: CTGGGTACCAGCTGCTAGCAAGCTTGCTAGCgccacc ATGGAATTGCATCAGGGCGAACG	This paper	N/A
Primer: SERT Reverse: CTGATCAGCGGGTTTAAACGGGCCCTCTCTCCTATC ATTTCCCGTCTATCAACCTGG	This paper	N/A
Recombinant DNA		
Plasmid for expression of SERT wild type	This paper	Addgene Plasmid #190743

REAGENT or RESOURCE	SOURCE	IDENTIFIER
Plasmid for expression of SERT C109A_Y107C mutant	Jacobs et al., 2007	Addgene Plasmid #190174
Plasmid for expression of SERT X5C_S277C mutant	Zhang and Rudnick, 2006	Addgene Plasmid #190177
Fab15B8 Heavy chain	Coleman et al., 2019	N/A
Fab15B8 Light chain	Coleman et al., 2019	N/A
SERT	UniProt: P31645	N/A
MSPNW11	Nasr et al., 2017	Laboratory of Gerhard Wagner
Plasmid: pcDNA3.1-zeocin-TetO	This paper	N/A
Plasmid: pcDNA3.4	Thermo Fisher Scientific	Cat# A14697
Software and algorithms		
Serial EM	Mastronarde, 2003	https://structura.bio/
DOCK 3.7	UCSF	https://dock.compbio.ucsf.edu/DOCK3.7/
DOCK Blaster	UCSF	https://blaster.docking.org/
ZINC20	UCSF	https://zinc20.docking.org/
CryoSparc v3.2.0	Structura Biotechnology	https://structura.bio/
Relion v.3.0	Zivanov et al., 2018	https://www3.mrc-lmb.cam.ac.uk/relion/index.php/Main_Page
Pyem v0.5	Asarnow et al., 2019	https://github.com/asarnow/pyem
dFSC	Dang et al., 2017	N/A
UCSF ChimeraX v1.4	Goddard et al., 2018	
ISOLDE	Croll, 2018	https://isolde.cimr.cam.ac.uk/
Phenix v1.20.1	Adams et al., 2010	http://www.phenix-online.org/
SPSS Statistics 27	IBM	https://www.ibm.com/products/spss-statistic
Prism 9.5.1	GraphPad	https://www.graphpad.com/scientific-software/prism/
GraphPad Prism v9	GraphPad Software	https://www.graphpad.com
Origin 2022b	OriginLab Corp.	https://www.originlab.com/
Other		
Q5 High-Fidelity 2X Master Mix	New England Bio-Labs	Cat# M0492
NucleoBond Xtra Midi Plus kit	Macherey-Nagel	Cat# 740412.50
ExpiFectamine 293 Transfection Kit	Thermo Fisher Scientific	Cat# A14524
Holey Gold Supports: UltrAuFoil (R 1.2/1.3) Au300 mesh	Quantifoil Micro Tools	N1-A14nAu30-01
Titan Krios Gi3	Thermo Fisher Scientific	N/A
BioQuantum Energy Filter	Gatan	N/A
K3 Direct Electron Detector	Gatan	N/A
Mouse Tail Suspension apparatus	Med Associates	MED-TSS-MS
Shuttle Box apparatus	Med Associates	MED-APA-D1M
Pulse Ultra Bright LED Strobe Light with 108 LEDs	Roxant or Amazon.com	
Holder and Bottles for anhedonia testing	Animal Care Systems	C79125A
Open Field	Omnitech Electronics	VersaMax Legacy System

REAGENT or RESOURCE	SOURCE	IDENTIFIER
Fear-Potentiated Startle apparatus (shock threshold)	Med Associates	MED-ASR-PRO1 MED-ASR-FPS